AUTOPHAGY
2023, VOL. 19, NO. 5, 1562–1581
https://doi.org/10.1080/15548627.2022.2140558

Taylor & Francis
Taylor & Francis Group

RESEARCH PAPER

PTP4A2 promotes lysophagy by dephosphorylation of VCP/p97 at Tyr805

Yunpeng Bai[a], Guimei Yu[a], Hong-Ming Zhou[b], Ovini Amarasinghe[c], Yuan Zhou[d], Peipei Zhu[c], Qinglin Li[a], Lujuan Zhang[e], Frederick Nguele Meke[a], Yiming Miao[a], Eli Chapman[f], W. Andy Tao[c,d,g], and Zhong-Yin Zhang[a,c,g,h*]

[a]Department of Medicinal Chemistry and Molecular Pharmacology, Purdue University, West Lafayette, USA; [b]Department of Dermatology, Indiana University School of Medicine, Indianapolis, IN, USA; [c]Department of Chemistry, Purdue University, West Lafayette, USA; [d]Department of Biochemistry, Purdue University, West Lafayette, USA; [e]Department of Speech, Language, and Hearing Sciences, Purdue University, West Lafayette, IN, USA; [f]Department of Pharmacology and Toxicology, University of Arizona, Tucson, A, USA; [g]Center for Cancer Research; [h]Institute for Drug Discovery, Purdue University, West Lafayette, IN, USA

ABSTRACT

Overexpression of PTP4A phosphatases are associated with advanced cancers, but their biological functions are far from fully understood due to limited knowledge about their physiological substrates. VCP is implicated in lysophagy via collaboration with specific cofactors in the ELDR complex. However, how the ELDR complex assembly is regulated has not been determined. Moreover, the functional significance of the penultimate and conserved Tyr805 phosphorylation in VCP has not been established. Here, we use an unbiased substrate trapping and mass spectrometry approach and identify VCP/p97 as a *bona fide* substrate of PTP4A2. Biochemical studies show that PTP4A2 dephosphorylates VCP at Tyr805, enabling the association of VCP with its C-terminal cofactors UBXN6/UBXD1 and PLAA, which are components of the ELDR complex responsible for lysophagy, the autophagic clearance of damaged lysosomes. Functionally, PTP4A2 is required for cellular homeostasis by promoting lysophagy through facilitating ELDR-mediated K48-linked ubiquitin conjugate removal and autophagosome formation on the damaged lysosomes. Deletion of *Ptp4a2 in vivo* compromises the recovery of glycerol-injection induced acute kidney injury due to impaired lysophagy and sustained lysosomal damage. Taken together, our data establish PTP4A2 as a critical regulator of VCP and uncover an important role for PTP4A2 in maintaining lysosomal homeostasis through dephosphorylation of VCP at Tyr805. Our study suggests that PTP4A2 targeting could be a potential therapeutic approach to treat cancers and other degenerative diseases by modulating lysosomal homeostasis and macroautophagy/autophagy.

Abbreviations: AAA+: ATPases associated with diverse cellular activities; AKI: acute kidney injury; CBB: Coomassie Brilliant Blue; CRISPR: clustered regularly interspaced short palindromic repeats; ELDR: endo-lysosomal damage response; GFP: green fluorescent protein; GST: glutathione S-transferase; IHC: immunohistochemistry; IP: immunoprecipitation; LAMP1: lysosomal-associated membrane protein 1; LC-MS: liquid chromatography-mass spectrometry; LGALS3/Gal3: galectin 3; LLOMe: L-leucyl-L-leucine methyl ester; MAP1LC3/LC3: microtubule associated protein 1 light chain 3; MEF: mouse embryonic fibroblast; PLAA: phospholipase A2, activating protein; PTP4A2: protein tyrosine phosphatase 4a2; PUB: NGLY1/PNGase/UBA- or UBX-containing protein; PUL: PLAP, Ufd3, and Lub1; TFEB: transcription factor EB; UBXN6/UBXD1: UBX domain protein 6; UPS: ubiquitin-proteasome system; VCP/p97: valosin containing protein; VCPIP1: valosin containing protein interacting protein 1; YOD1: YOD1 deubiquitinase.

ARTICLE HISTORY
Received 25 January 2022
Revised 21 October 2022
Accepted 21 October 2022

KEYWORDS
Autophagy; dephosphorylation; ELDR complex; lysosome; PLAA; PRL phosphatase; PTP4A2; UBXN6; VCP

Introduction

Protein tyrosine phosphorylation is essential for proper cellular operation. Abnormalities in protein tyrosine phosphorylation contribute to many human disorders. Given the success in halting disease progression through inhibition of protein tyrosine kinase activity [1], improved understanding of the biological underpinnings of protein tyrosine phosphatases (PTPs) is expected to create new opportunities for targeted disease intervention. Among the >100 members of the PTP superfamily are PTP4A1 (protein tyrosine phosphatase 4a1) PTP4A2 and PTP4A3, which are highly oncogenic when overexpressed [2–4]. Aberrantly high PTP4A expression promotes cell proliferation, migration, and tumorigenesis *in vivo* [5–11]. Elevated PTP4A level is observed in many types of tumors and is strongly correlated with late-stage metastasis and poor clinical outcomes [2,4,12,13]. These findings identify PTP4As as potential therapeutic targets for metastatic cancers.

In spite of the oncogenicity associated with PTP4A overexpression, their fundamental roles in normal cellular physiology and tumor development are not completely understood. Previous studies have shown that ectopic expression of PTP4As in cultured cells leads to activation of several signaling molecules, including the RHO family of small GTPases, SRC, STAT3, MAPK1/ERK2-MAPK3/ERK1, and AKT [3]. PTP4As are also reported to interact with the CNNM family of magnesium transport mediators and

CONTACT Zhong-Yin Zhang zhang-zy@purdue.edu Department of Medicinal Chemistry and Molecular Pharmacology, West Lafayette, IN 47907, USA
*Lead contact

Supplemental data for this article can be accessed online at https://doi.org/10.1080/15548627.2022.2140558

regulate intracellular Mg^{2+} concentration [14]. Mice deficient in *Ptp4a2*, the most abundantly and ubiquitously expressed PTP4A family member, display several developmental anomalies, due to increased level of PTEN and decreased AKT activity in the affected tissues [15–17]. Notably, *Ptp4a2* deletion in *Pten* heterozygous mice (*ptp4a2*$^{-/-}$) raises the PTEN level, reduces AKT activity, and impedes *Pten* deficiency-induced tumorigenesis [18]. Mechanistic analysis reveals that PTP4A2 downregulates PTEN and promotes tumorigenesis by dephosphorylating PTEN at Tyr336, which augments the NEDD4-mediated PTEN ubiquitination for proteasomal degradation [18]. Interestingly, a critical role of autophagy in PTP4A3-driven tumor progression has also been reported [19], although the underlying mechanism has not been fully elucidated. Therefore, continued identification and characterization of PTP4A substrates will enhance our understanding of the PTP4As in normal and disease biology.

Autophagy is a tightly regulated lysosome-mediated intracellular degradative process that removes and recycles dysfunctional cellular components such as damaged organelles and misfolded proteins [20]. Defects in autophagy have been linked to cancer and neurodegenerative disorders [21]. Proper function and integrity of lysosomes are therefore essential for normal cellular functions. Given the absolute requirement of lysosome for autophagy and detrimental consequences from unwanted leakage of lysosomal content to the cellular milieu, lysosomal damage poses severe threat to cellular well-being [22]. Lysophagy, a specific type of selective autophagy, clears damaged lysosomes through the autophagic process [23–25]. VCP/p97 (valosin containing protein), an evolutionarily conserved cytosolic member of the ATPases Associated with diverse cellular Activities (AAA+), is a master regulator of cellular homeostasis [26,27]. Although best known for its role as a protein "segregase" that extracts and unfolds ubiquitinated substrates from protein complexes or membranes for proteasomal degradation [27,28], VCP also serves as a crucial regulator of selective autophagy, including lysophagy [29–33]. To that end, an endo-lysosomal damage response (ELDR) complex, consisting of VCP and its cofactors UBXN6/UBXD1 (UBX domain protein 6), PLAA (phospholipase A2, activating protein), and YOD1 (YOD1 deubiquitinase), was recently identified as essential machinery for the detection and clearance of ruptured lysosomes by lysophagy [31]. However, the mechanism by which the ELDR complex assembly is regulated is still unknown. Here, we identify VCP as a novel substrate of PTP4A2 by substrate trapping and mass spectrometry. We further demonstrate that dephosphorylation of VCP at the penultimate and conserved Tyr805 by PTP4A2 promotes the association of VCP with its C-terminal cofactors UBXN6 and PLAA, therefore facilitating autophagosome formation and clearance of damaged lysosomes. Downregulation of PTP4A2 impairs the ELDR complex assembly, leading to prolonged lysosomal damage. Importantly, deletion of *Ptp4a2* in mice delays the recovery from acute kidney injury (AKI) due to prolonged lysosomal damage. Taken together, our study reveals an essential role for PTP4A2 in promoting VCP-mediated lysophagy to maintain cellular homeostasis.

Results

Identification of VCP as a PTP4A2 substrate

To further define the biochemical basis for PTP4A functions, we sought to identify and characterize physiological substrates for the PTP4A phosphatases. We used a catalytically inactive PTP4A2 substrate-trapping mutant PTP4A2^{D69A,C101S} [18], hereinafter referred to as PTP4A2 [DACS], to capture its substrates from human acute myeloblastic leukemia Kasumi-1 cell treated with pervanadate, a pan-PTP inhibitor. One of the prominent tyrosine-phosphorylated proteins at ~95 kDa was found specifically bound to GST (glutathione S-transferase)-tagged PTP4A2[DACS] in both the elution and glutathione beads fraction, but not the GST control or GST-PTP4A2 (Figure 1A). The 95-kDa band was also consistently identified as the major tyrosine-phosphorylated protein from human chronic myelogenous leukemia K562 (Figure S1A) and immortalized mouse spermatocyte GC-1 cells (Figure S1C). We then performed an in-gel digestion of the 95-kDa band from Kasumi-1 and K562 cells for protein identification by liquid chromatography-mass spectrometry (LC-MS). VCP surfaced as a top hit and a putative PTP4A2 substrate based on the LC-MS analyses (Figure 1B and S1B). To demonstrate the robustness of the substrate trapping and mass spectrometry identification approach, we also compared the 95-kDa fractions from both the GST-PTP4A2[DACS] and GST-PTP4A2 bound samples from GC-1 cells, which were reduced, alkylated and proteolytically digested by trypsin for mass spectrometric sequencing. VCP was identified only from the GST-PTP4A2[DACS] captured sample, but not from GST-PTP4A2 (Figure S1D). To corroborate the mass spectrometry results, a VCP specific antibody was used to directly detect VCP in the substrate trapping samples. As expected, VCP was pulled down by GST-PTP4A2 [DACS], but not GST-PTP4A2 or GST alone, from the K562, Kasumi-1, human histiocytic lymphoma U937 and human acute promyelocytic leukemia HL-60 cell lysates (Figure 1C). Moreover, we also generated a plasmid of green fluorescent protein (GFP) tagged VCP and co-expressed it with Flag-PTP4A2 or Flag-PTP4A2[DACS] in HEK293 cells. Not surprisingly, GFP-VCP was strongly trapped by GST-PTP4A2[DACS] or Flag-PTP4A2[DACS] as a tyrosine-phosphorylated protein (Figure 1D and 1E).

To further verify VCP as a PTP4A2 substrate, we assessed the ability of PTP4A2 to directly dephosphorylate VCP. Recombinant His-tagged PTP4A2 protein, but not the catalytically inactive PTP4A2^{C101S} mutant, reduced the overall tyrosine-phosphorylation of immunoprecipitated VCP from either human embryonic kidney (HEK) 293 or human breast adenocarcinoma MCF7 cells (Figure 2A and 2B). It is noteworthy that the phosphatase activity exhibited by PTP4A2 toward VCP is comparable to that of PTP1B, a member of the PTP family with robust phosphatase activity (Figure S2A and S2B). Furthermore, co-expression of HA-PTP4A2 and Flag-VCP in human lung carcinoma

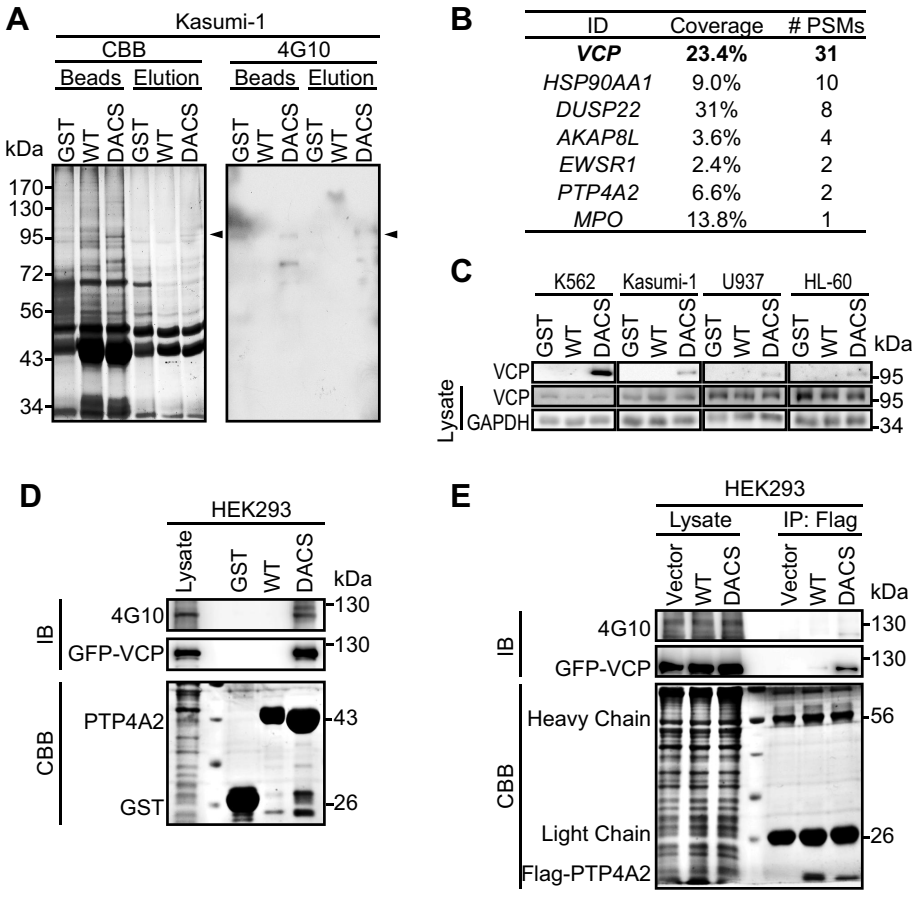

Figure 1. Identification of VCP as a PTP4A2 substrate. (**A**). Substrate trapping by GST affinity isolation was done by incubating lysates from pervanadate-treated Kasumi-1 cells with GST, GST-PTP4A2 and GST-PTP4A2[DACS] beads. The bound proteins were eluted with pervanadate, and both elution and remaining beads were fractionated by SDS-PAGE, and stained by Coomassie Brilliant Blue or blotted with phosphotyrosine antibody (4G10). (**B**). In-gel digestion of the p95 band from Kasumi-1 cells for protein identification by LC-MS, and VCP was identified as the top hit as PTP4A2 substrate. (**C**). PTP4A2 substrate trapping by GST affinity isolation. Pervanadate-treated K562, Kasumi-1, U937 and HL-60 cell lysates were incubated with GST, GST-PTP4A2 and GST-PTP4A2[DACS] beads. The affinity isolated proteins and the lysate were blotted with VCP and GAPDH antibodies. (**D**). Pervanadate-treated GFP-VCP-expressing HEK293 cell lysates were incubated with GST, GST-PTP4A2 and GST-PTP4A2[DACS] beads. The bound proteins were blotted with phosphotyrosine (4G10) and GFP antibodies, and stained by Coomassie Brilliant Blue to reveal the amount of GST proteins. (**E**). Flag-PTP4A2 or Flag-PTP4A2[DACS] were co-expressed with GFP-VCP in HEK293 cells, then Flag-IP was performed for substrate trapping. The bound proteins were blotted with phosphotyrosine (4G10) and GFP antibodies, and stained by Coomassie Brilliant Blue to reveal the amount of immunoprecipitated PTP4A2 proteins. CBB: Coomassie Brilliant Blue; IB: immunoblot; IP: immunoprecipitation.

H1299 cells considerably diminished the overall tyrosine phosphorylation on VCP (Figure 2C). These data indicate that PTP4A2 can dephosphorylate VCP on tyrosine residues(s) *in vitro* and inside the cells. We further established that, in addition to PTP4A2, co-expression of either HA-PTP4A1 or HA-PTP4A3 with Flag-VCP also reduced the overall phosphorylation on VCP (Figure S2C), indicating that VCP is likely a substrate for all PTP4As. We next examined whether PTP4A2 can dephosphorylate endogenous VCP inside the cell. As shown in Figure 2D and 2E, Flag-PTP4A2 expression substantially reduced endogenous VCP tyrosine phosphorylation in both HEK293 and H1299 cells. In contrast, clustered regularly interspaced short palindromic repeats (CRISPR)-mediated *PTP4A2* deletion in MCF7 cells notably enhanced VCP tyrosine phosphorylation (Figure 2F). These observations show that PTP4A2 can dephosphorylate endogenous VCP on tyrosine residue(s). Taken together, the results identify VCP as a novel PTP4A2 substrate.

PTP4A2 dephosphorylates VCP at its penultimate tyrosine 805

Phosphorylation of the penultimate Tyr805 at the C terminus of VCP has been reported to account for more than 90% of the overall VCP tyrosine phosphorylation [34]. Tyr805 is strictly conserved among VCPs from different species (Figure S3A), indicating an evolutionarily conserved function for Tyr805 phosphorylation of VCP. To determine if PTP4A2-mediated VCP dephosphorylation occurs at its C terminus, we generated a series of truncated Flag-VCP constructs, including VCP[[1–48]], VCP[[1–76]], VCP[209–806], and VCP[482–806] (Figure S3B). We found that the truncated VCP constructs could still be tyrosine phosphorylated if the C-terminal segment (762–806) was intact, and that expression of PTP4A2 significantly inhibited VCP tyrosine phosphorylation, indicating that PTP4A2 dephosphorylates VCP C-terminal tyrosine residues (Figure S3B and S3C).

We next performed mass spectrometry analyses to determine the site and extent of VCP dephosphorylation by

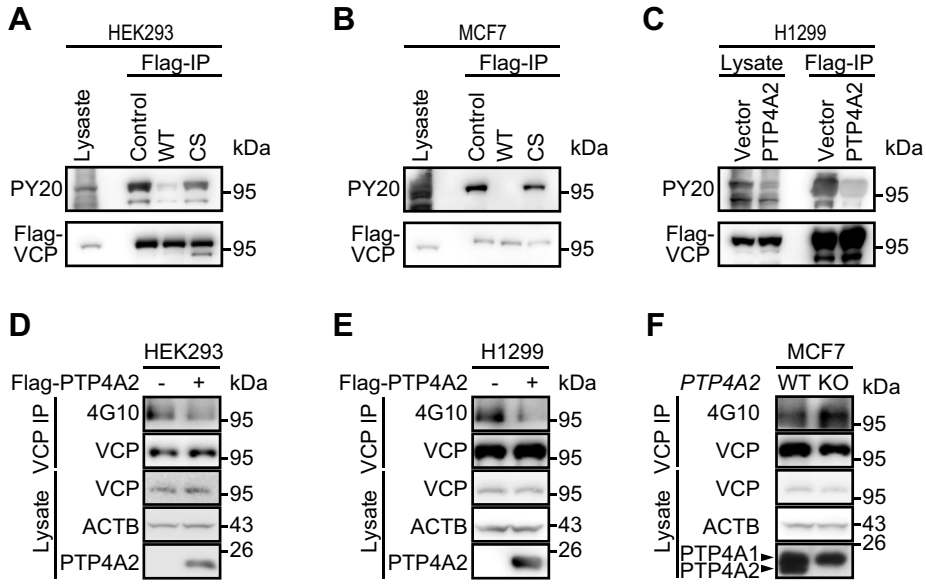

Figure 2. PTP4A2 dephosphorylates tyrosine phosphorylated VCP. (**A** and **B**). His-PTP4A2 dephosphorylates immunoprecipitated Flag-VCP from cells. Incubation of 5 μM purified His-tagged PTP4A2 or its inactive mutant PTP4A2^{C101S} with 5 μM of immunoprecipitated Flag-VCP from either HEK293 cells (**A**) or MCF7 cells (**B**) for 1 h, then dephosphorylation of VCP was examined by blotting with phosphotyrosine (PY20) and Flag antibodies. (**C**). HA-PTP4A2 and Flag-VCP were co-expressed in H1299 cells, and Flag-IP was performed. The lysate and bound proteins were blotted with phosphotyrosine (PY20) and Flag antibodies. (**D** and **E**). Flag-PTP4A2 was overexpressed in HEK293 (**D**) or H1299 (**E**) cells, and VCP-IP was performed. The lysate and bound proteins were blotted with phosphotyrosine (4G10), VCP, ACTB and Flag antibodies. (**F**). CRISPR-Cas9-mediated *PTP4A2* deletion was carried out, and VCP-IP was performed in MCF7 cells. The lysate and bound proteins were blotted with phosphotyrosine (4G10), VCP, ACTB, PTP4A1 and PTP4A2 antibodies. IP: immunoprecipitation.

PTP4A2 with stable isotope dimethyl labeling of Flag-VCP in vector control and HA-PTP4A2-expressing cells (Figure 3A-C). We confirmed successful immunoprecipitation (IP) of VCP by Coomassie Brilliant Blue (CBB) staining (Figure S3D) and found that PTP4A2 expression reduced VCP tyrosine phosphorylation by 60% (Figure 3B). The immunoprecipitated VCP samples were trypsin digested on-beads, and stable-isotope dimethyl labeling was performed on VCP peptides from both vector control group (light, $^{12}CH_2O$) and HA-PTP4A2 co-expressing group (heavy, $^{13}CD_2O$). The same amount of peptides from control and HA-PTP4A2 overexpressing H1299 cells were pooled together for a total of 3 replicates for IMAC enrichment (95% pooled sample) followed by LC-MS/MS. To identify the site of VCP dephosphorylation upon PTP4A2 expression, we searched for phosphorylation sites (>2-fold decrease; $p < 0.05$) on VCP. A total of 21 phosphorylation sites were identified, and quantitative LC-MS/MS analysis revealed that only the phosphorylation of Tyr805 showed more than 50% reduction upon PTP4A2 expression (Figure 3C and S3E). These findings suggest that the C-terminal Tyr805 was specifically dephosphorylated by PTP4A2. To further confirm this result, we measured VCP phosphorylation in either WT or *Ptp4a2*-deficient mouse embryonic fibroblast (MEF) cells (Figure 3D-F). Endogenous VCP was successfully immunoprecipitated from these cells (Figure S3F), and western blot showed that VCP was highly tyrosine phosphorylated in *ptp4a2*-deleted MEF cells (Figure 3E). Quantitative LC-MS /MS measurements were then performed, and Tyr805 was the only site of phosphorylation identified in endogenous VCP. In line with the mass spectrometry data from HA-PTP4A2 overexpressing H1299 cells (Figure 3C), we found a ~ 2.5-fold increase in Tyr805 phosphorylation in *ptp4a2*-deleted MEF cells (Figure 3F), further demonstrating that PTP4A2 catalyzes VCP dephosphorylation on Tyr805.

To further study the PTP4A2-catalyzed VCP dephosphorylation at Tyr805, we generated a phospho-specific antibody p-VCP (Tyr805) against this site using VCP C-terminal phosphopeptide CSVYTEDNDDDLpYG (VCP [p-Tyr805] peptide) as an antigen. To characterize the p-VCP (Tyr805) antibody, we prepared recombinant VCP with site-specific phosphorylation at Tyr805 (VCP [p-Tyr805] protein) by expressed protein ligation [35] (Figure S3G and S3H). To evaluate the specificity of the p-VCP (Tyr805) antibody, we utilized the ligated VCP (p-Tyr805) protein as a positive control and the bacterially expressed recombinant VCP as a negative control in a Phos-tag gel assay, which can differentiate up-shifted phosphorylated proteins from non-phosphorylated counterparts. As expected, the p-VCP (Tyr805) antibody specifically recognized the ligated VCP (p-Tyr805) protein but not the non-phosphorylated VCP sample (Figure S3I). In addition, treatment of the ligated VCP (p-Tyr805) protein with PTP1B completely abolished the p-Tyr805 signal, leading to a downshift band of the ligated VCP (p-Tyr805). Consistent with previous findings that VCP Tyr805 is phosphorylated by the SRC kinase [36,37], we confirmed that SRC can indeed phosphorylate the full-length VCP at Tyr805, since little tyrosine phosphorylation was observed in VCP [1–795] in the presence of SRC (Figure S3J). We also found that pervanadate treatment significantly enhanced the p-Tyr805 signal in H1299 cells overexpressing Flag-VCP (Figure S3K). Collectively, these results indicate that we have successfully obtained a specific antibody against Tyr805-phosphorylated VCP.

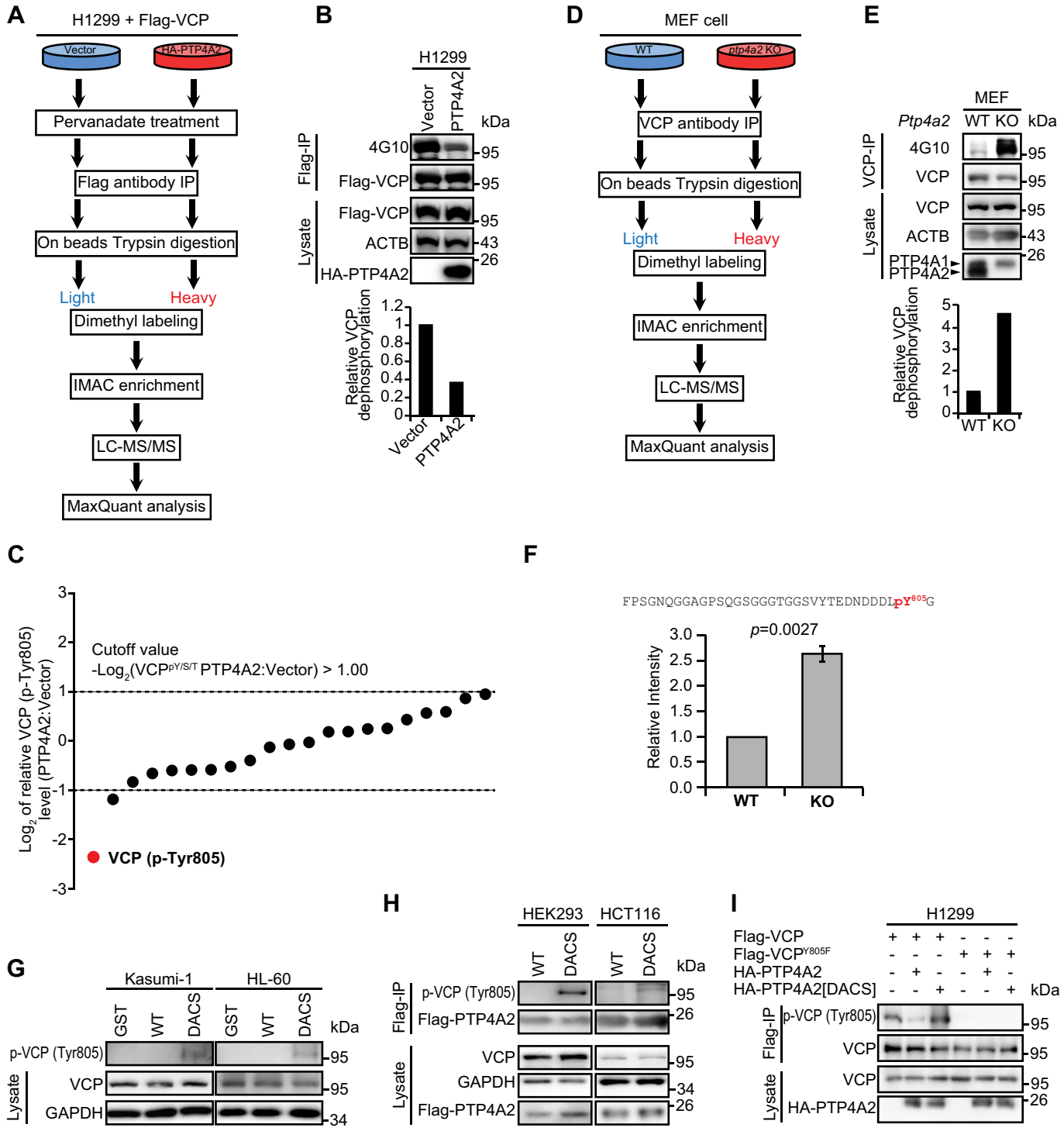

Figure 3. Tyr805 of VCP is dephosphorylated by PTP4A2. (**A**). Experimental design of quantitative LC-MS/MS analysis by stable isotope dimethyl labeling to identify the sites that PTP4A2 dephosphorylates on VCP in H1299 cells overexpressing Flag-VCP with or without HA-PTP4A2. (**B**). HA-PTP4A2 and Flag-VCP were co-expressed in H1299 cells, and Flag-IP was performed. The lysate and bound proteins were blotted with phosphotyrosine (4G10), Flag, ACTB and HA antibodies. The reduction of relative VCP phosphorylation upon PTP4A2 overexpression in H1299 cells was quantified based on the intensity of the bands by ImageJ. (**C**). The relative fold change of all the phosphorylation sites (including Ser-, Thr- and Tyr-phosphorylation) identified on VCP by LC-MS/MS. A total of 21 phosphorylation sites were identified, and the red dot is Tyr805. (**D**). Experimental design of quantitative LC-MS/MS analysis by stable isotope dimethyl labeling to identify the sites that PTP4A2 dephosphorylates on VCP in WT and *ptp4a2*-deficient MEF cells. (**E**). VCP-IP was performed in WT and *ptp4a2* KO MEF cells. The lysate and bound proteins were blotted with phosphotyrosine (4G10), VCP, ACTB and PTP4A1 and PTP4A2 antibodies. The reduction of relative VCP phosphorylation upon *ptp4a2* deletion in MEF cells was quantified based on the intensity of the bands by ImageJ. (**F**). The relative fold change of VCP Tyr805 phosphorylation in WT and *ptp4a2* KO MEF cells by LC-MS/MS. (**G**). PTP4A2 substrate trapping by GST affinity isolation. Pervanadate-treated Kasumi-1 or HL-60 cell lysates were incubated with GST, GST-PTP4A2 and GST-PTP4A2[DACS] bound on beads. The lysate and bound proteins were blotted with p-VCP (Tyr805), VCP and GAPDH antibodies. (**H**). PTP4A2 substrate trapping by Flag-IP. Flag-PTP4A2 or PTP4A2[DACS] was transiently transfected into HCT116 and HEK293 cells, and then Flag-IP was performed after pervanadate treatment. The lysate and bound proteins were blotted with p-VCP (Tyr805), VCP, GAPDH and Flag antibodies. (**I**). HA-PTP4A2 dephosphorylates Flag-VCP in H1299 cells. HA-PTP4A2 or PTP4A2[DACS] was co-expressed with Flag-VCP or VCP^{Y805F} in H1299 cells, and then Flag-IP was performed after pervanadate treatment. The lysate and bound proteins were blotted with p-VCP (Tyr805) specific, VCP and HA antibodies. IP: immunoprecipitation.

We then utilized the p-VCP (Tyr805) specific antibody to investigate the PTP4A2-catalyzed VCP dephosphorylation. Substrate trapping experiments confirmed that Tyr805 phosphorylated VCP was indeed associated with PTP4A2[DACS] in different cell lines (Figure 3G and 3H). Furthermore, co-expressing PTP4A2, but not its inactive mutant PTP4A2 [DACS], with VCP in H1299 cells significantly reduced VCP Tyr805 phosphorylation level, whereas the VCP^{Y805F} mutant did not show any reactivity with the p-VCP (Tyr805) antibody (Figure 3I). To quantitatively determine the specificity and efficiency of PTP4A2 mediated dephosphorylation of VCP at Tyr805, we performed PTP4A2 phosphatase assay using both the ligated VCP (p-Tyr805) protein (Figure S3L) and VCP C-terminal p-Tyr805 containing peptide CSVYTEDNDDDL(pY)G as substrates (Figure S3M). We found the catalytic efficiency (k_{cat}/K_M) for the PTP4A2-catalyzed hydrolysis of VCP (p-Tyr805) protein (165.9 ± 15.3 $M^{-1}s^{-1}$) is 186- and 263-fold higher than those of *p*NPP (0.89 ± 0.06 $M^{-1}s^{-1}$) and VCP C-terminal p-Tyr805 peptide (0.63 ± 0.05 $M^{-1}s^{-1}$), respectively. These data further demonstrate that PTP4A2 specifically dephosphorylates Tyr805 at the C terminus of VCP.

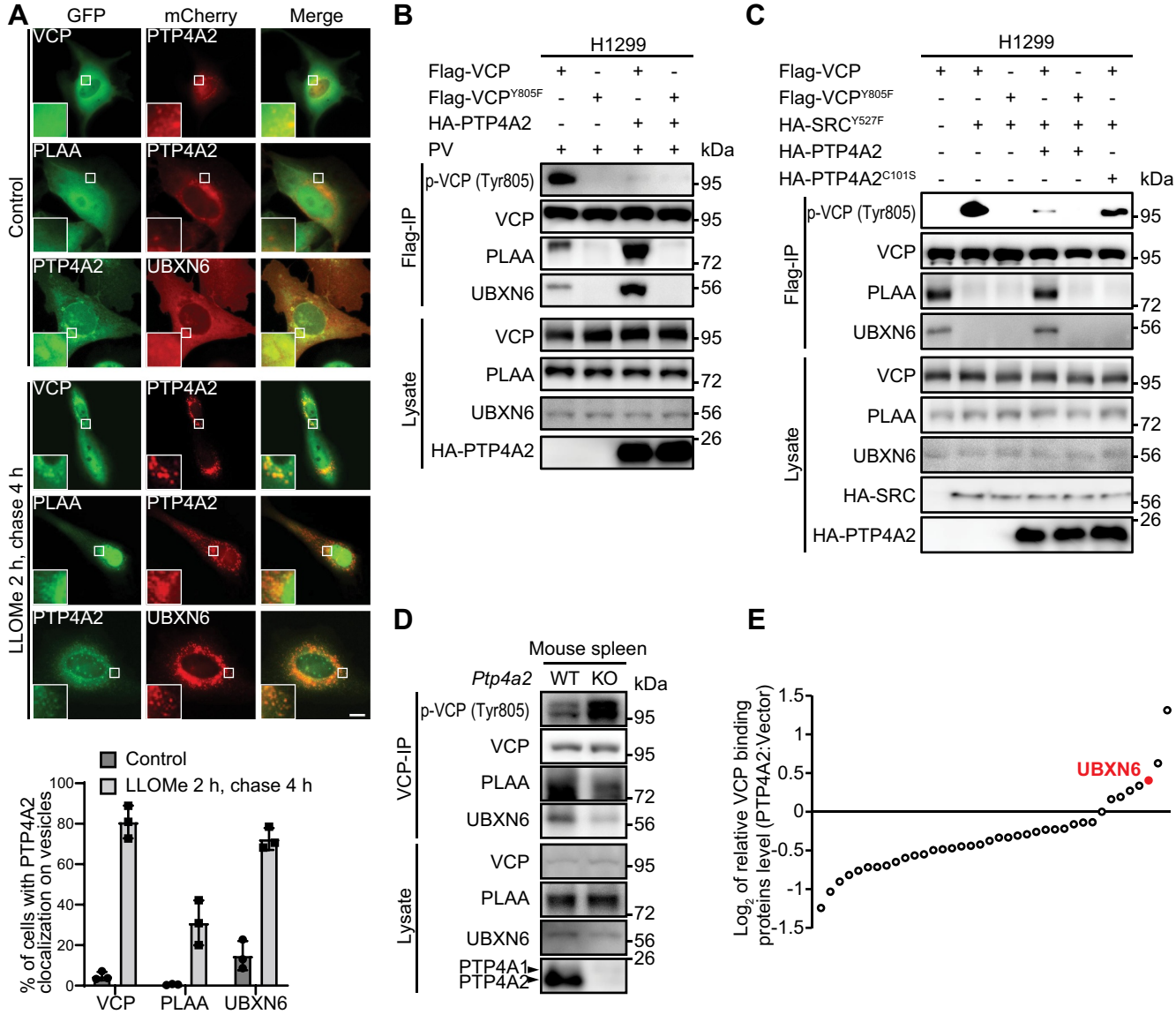

Figure 4. PTP4A2-mediated dephosphorylation of VCP at Tyr805 enhances the interaction between VCP and its C-terminal cofactors. (**A**). GFP-VCP and GFP-PLAA, or mCherry-UBXN6 was co-expressed with mCherry-PTP4A2 or GFP-PTP4A2 in U2OS cells for 24 h, and then treated with or without 250 μM LLOMe for 2 h. Cells were washed and replaced with fresh medium for 4 h, and then cells were fixed and GFP and mCherry signals were captured by microscope. The bar graph represents the percentage of cells with PTP4A2 colocalization on vesicles. Scale bar: 10 μm. (**B**). HA-PTP4A2 was co-expressed with Flag-VCP or VCP^{Y805F} in H1299 cells, and then Flag-IP was performed after pervanadate treatment. The lysate and bound proteins were blotted with p-VCP (Tyr805) specific, VCP, PLAA, UBXN6 and HA antibodies. (**C**). HA-PTP4A2 or $PTP4A2^{C101S}$ was co-expressed with HA-Src^{Y527F} and Flag-VCP or VCP^{Y805F} in H1299 cells, and then Flag-IP was performed. The lysate and bound proteins were immunoblotted with p-VCP (Tyr805) specific, VCP, PLAA, UBXN6 and HA antibodies. (**D**). Mouse spleen was isolated from WT or *ptp4a2* KO mice, and VCP-IP was performed. The lysate and bound proteins were blotted with p-VCP (Tyr805) specific, VCP, PLAA, UBXN6 and PTP4A1 and PTP4A2 antibodies. (**E**). The relative fold change of all VCP binding proteins by LC-MS/MS. A total of 38 proteins were identified, and the red dot is UBXN6. IP: immunoprecipitation. PV: pervanadate.

PTP4A2 catalyzed VCP dephosphorylation at Tyr805 promotes ELDR complex formation

The C-terminal tail of VCP is known to bind NGLY1/PNGase/UBA- or UBX-containing proteins (PUB) or the PLAP, Ufd3, and Lub1 (PUL) domain [37–40]. Interestingly, mutations of the strictly conserved Tyr805 in VCP, even a subtle change from Tyr to Phe, completely abolished the VCP-PUB and VCP-PUL interaction [36,37]. Moreover, phosphorylation of Tyr805 by SRC also abolishes the interaction between VCP and PUB or PUL domain-containing proteins [36,37]. These observations highlight the importance of the hydroxyl group on Tyr805 for PUB and PUL interactions. However, the functional significance of VCP Tyr805 phosphorylation has not been established. We hypothesized that PTP4A2 promotes the ELDR complex assembly through dephosphorylation of VCP at Tyr805.

To define the functional role of PTP4A2-mediated VCP Tyr805 dephosphorylation, we first examined the colocalization of PTP4A2 with VCP and its C-terminal co-factors PLAA and UBXN6 inside the cell. As shown in Figure 4A, PTP4A2 colocalized with VCP, PLAA and UBXN6 in punctate structures within the cell upon lysosomal damage. Of Note, PTP4A1 and PTP4A3 also colocalized with VCP puncta when treated with lysosomal damage reagent L-leucyl-L-leucine methyl ester (LLOMe) (Figure S4A). We also found that LLOMe does not affect PTP4A2's phosphatase activity toward the VCP (p-Tyr805) protein (Figure S4B), indicating that PTP4A activities are not sensitive to lysosome damage. Importantly, we found that PTP4A2-mediated dephosphorylation of Tyr805 increased UBXN6 and PLAA association with VCP (Figure 4B). Consistent with previous findings [36,37], substitution of Tyr805 by Phe completely abolished the interaction between VCP and UBXN6 or PLAA either in the presence or absence of PTP4A2 (Figure 4B). Furthermore, expression of the constitutively active SRC^{Y527F} significantly enhanced VCP Tyr805 phosphorylation and diminished VCP interaction with PLAA and UBXN6, while PTP4A2 but not its phosphatase dead mutant $PTP4A2^{C101S}$ abrogated SRC-mediated VCP phosphorylation and restored PLAA and UBXN6 association with VCP (Figure 4C). As expected, VCP^{Y805F} could not be phosphorylated by SRC^{Y527F} and is unable to interact with PLAA and UBXN6 with or without the presence of PTP4A2 (Figure 4C). These findings demonstrated that PTP4A2 reverses SRC-mediated Tyr805 phosphorylation on VCP and promotes PLAA and UBXN6 binding to VCP. To further confirm this conclusion *in vivo*, we immunoprecipitated VCP from spleen samples of either control or *ptp4a2*$^{-/-}$ mice and found that deletion of *Ptp4a2* not only enhanced VCP Tyr805 phosphorylation, but also reduced the level of PLAA and UBXN6 bound to VCP (Figure 4D). Taken together, our data suggest that PTP4A2-mediated dephosphorylation of VCP at Tyr805 promotes the interaction between VCP and its C-terminal cofactors PLAA and UBXN6, which are major components of the ELDR complex.

To further examine the changes in VCP binding proteins upon PTP4A2 expression, we also analyzed the total cellular proteomes between control and PTP4A2 expressing cells using stable isotope dimethyl labeling (Figure 3A). As described in previous section, immunoprecipitated Flag-VCP in the presence or absence of HA-PTP4A2 was digested with trypsin and the same amount of peptides from control and HA-PTP4A2 cells were pooled together (5% pooled sample) for a total of 3 replicates for proteome analysis to identify alterations in VCP binding proteins. Consistent with the biochemical analysis, VCP-bound UBXN6 showed more than a 30% increase in abundance ($p < 0.05$) upon PTP4A2 expression, although PLAA was not detected in this mass spectrometry experiment (Figure 4E). In addition, a list of known VCP-binding proteins or cofactors has been identified (Figure 4E and Table S1). Among them, 7 proteins showed increased interaction with VCP, while 30 proteins showed decreased interaction with VCP in PTP4A2 expressing cells. These data suggest that PTP4A2 catalyzed VCP Ty805 dephosphorylation not only changes C-terminal cofactor interaction but may also alter its overall cofactor binding profile. Further investigations are required to examine the physiological relevance of these additional alterations.

PTP4A2 is essential for autophagy-mediated clearance of damaged lysosomes

VCP coordinates with specific cofactors to regulate distinct cellular processes, including cell division, organelle biogenesis,

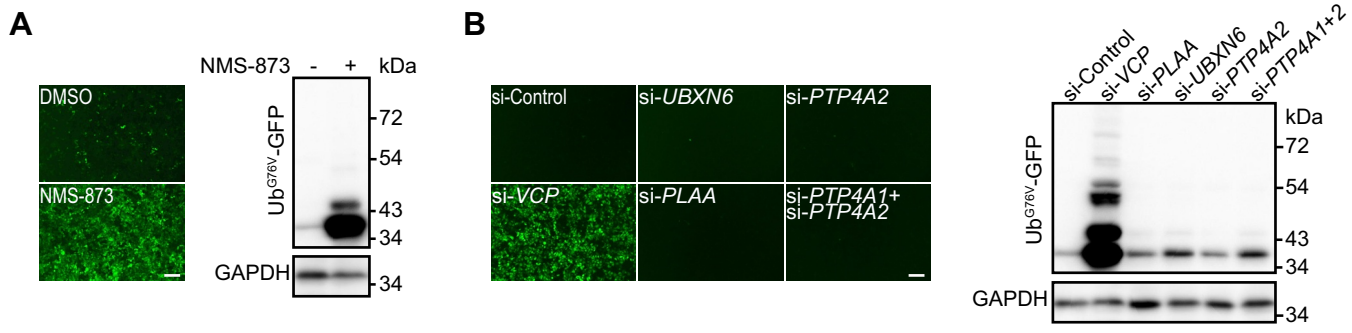

Figure 5. PTP4A2 is not involved in VCP-mediated UPS pathway. (**A**). Reporter cells stably expressing Ub^{G76V}-GFP was treated with 10 μM VCP inhibitor NMS-873 for 24 h, and GFP signal was captured by microscope and western blot. (**B**). Ub^{G76V}-GFP reporter cells were transfected with siRNAs (set 1) against *VCP, PLAA, UBXN6, PTP4A2* or *PTP4A1* for 72 h, and GFP signal was captured by microscope and western blot. Scale bars: 200 μm.

and protein degradation via the ubiquitin-proteasome system (UPS) [41]. To determine whether PTP4A2-catalyzed VCP Tyr805 dephosphorylation is involved in the VCP-mediated UPS pathway, we utilized a reporter cell line stably expressing Ub^{G76V}-GFP, a well-characterized ubiquitin fusion degradation reporter [42]. As a control, NMS-873, a selective allosteric inhibitor of VCP [43], successfully elevated the level of Ub^{G76V}-GFP (Figure 5A). To probe the potential involvement of PTP4A2 in the UPS pathway, we compared the Ub^{G76V}-GFP level upon siRNA mediated knockdown of either ELDR complex components or PTP4A family members. We confirmed that the two different sets of siRNAs (set 1 and set 2) used in the experiment could achieve at least 90% gene knockdown efficiency (Figure S5A and S5B). We showed that knockdown of *VCP* significantly enhanced the accumulation of Ub^{G76V}-GFP, in line with an essential role of VCP in UPS (Figure 5B and S5C). However, depletion of either *PLAA* or *UBXN6* did not affect the degradation of Ub^{G76V}-GFP,

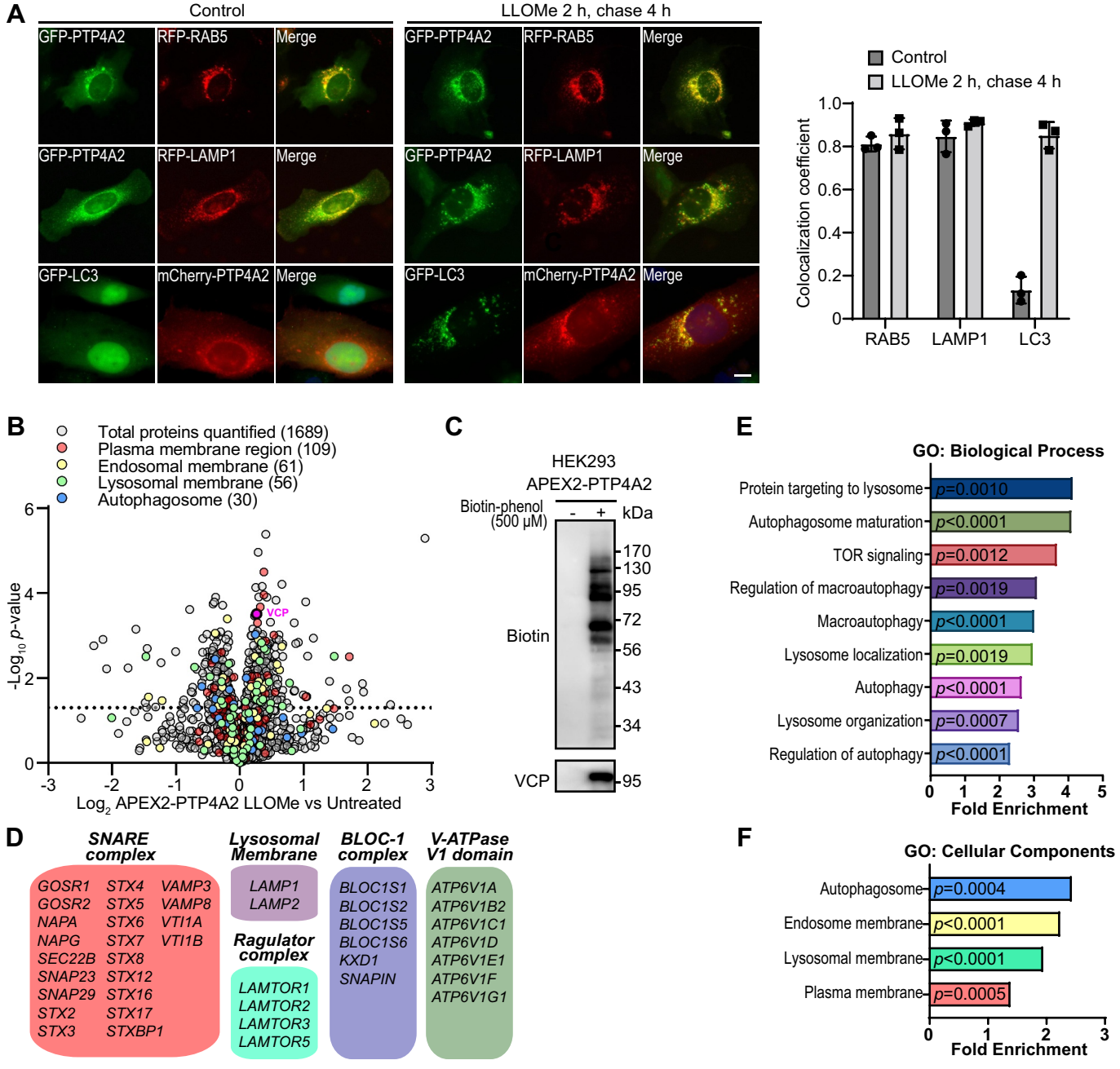

Figure 6. PTP4A2 is a lysosomal membrane protein. (**A**). GFP-PTP4A2 and RFP-Rab5 (endosome) or RFP-LAMP1 (lysosome), or mCherry-PTP4A2 and GFP-LC3 (autophagosome) were co-transfected into U2OS cells for 24 h, and then treated with or without 250 μM LLOMe for 2 h. Cells were washed and replaced with fresh medium for 4 h, and then cells were fixed and GFP and mCherry signals were captured by microscope. The bar graph represents the correlation coefficients for colocalization calculated by ImageJ JACoP plugin. Three independent experiments with at least 30 cells in each experiment were used for calculation. Scale bar: 10 μm. (**B**). Volcano plot for LLOMe (3 h)-treated APEX2-PTP4A2 stably expressing HEK293 cells versus untreated cells (Log_2 fold change versus – Log_{10} p-value) for APEX2-PTP4A2-based proximity labeling experiment. (**C**). The bound proteins from NeutrAvidin affinity isolation were immunoblotted with Biotin and VCP antibodies. (**D**) Summary of key lysosomal proteins or complexes found in PTP4A2 proteomics. (**E** and **F**) GO enrichment of Biological Process (**E**) and Cellular Components (**F**) for proteins that identified in PTP4A2 proximity.

indicating that the ELDR complex is not involved in UPS. Consistent with this notion, knockdown of *PTP4A2* or both *PTP4A1* and *PTP4A2* failed to raise Ub^{G76V}-GFP level (Figure 5B and S5C). These data indicate that PTP4A2-mediated VCP Tyr805 dephosphorylation is not involved in the UPS pathway.

In addition to its established role in UPS, VCP can also serve as an essential regulator of selective autophagy, including lysophagy [29–33]. A recent study has linked a function of VCP and its C-terminal cofactors to the clearance of ruptured lysosomes through autophagy, where VCP associates with UBXN6, PLAA and YOD1 to form an ELDR complex to remove K48-linked ubiquitin conjugates on damaged lysosomes and promote autophagosome formation for the clearance of damaged lysosomes [31]. Of note, we found here that dephosphorylation of VCP at Tyr805 by PTP4A2 is required for the ELDR complex formation (Figure 4 and Table S1), suggesting that PTP4A2 is required for autophagy-mediated damaged lysosome clearance. To further strengthen the functional linkage between PTP4A2 and lysophagy, we first examined the subcellular localization of PTP4A2. PTP4As possess a CAAX prenylation motif at their C terminus, which localizes them to the plasma membrane and the endosomal compartments [8,44–47]. In addition to endosome localization as previously reported [44–46], we found that PTP4A2 is also localized at lysosome and autophagosomes upon lysosomal damage as evidenced by its colocalization with LAMP1 (lysosomal-associated membrane protein 1) and MAP1LC3/LC3 (microtubule-associated protein 1 light chain 3) (Figure 6A). Similarly, PTP4A1 and PTP4A3 also showed lysosomal localization in both basal and lysosomal damage condition, and both colocalized with autophagosome upon lysosomal damage (Figure S6). To further support this observation, we performed an APEX2-PTP4A2 proximity labeling experiment

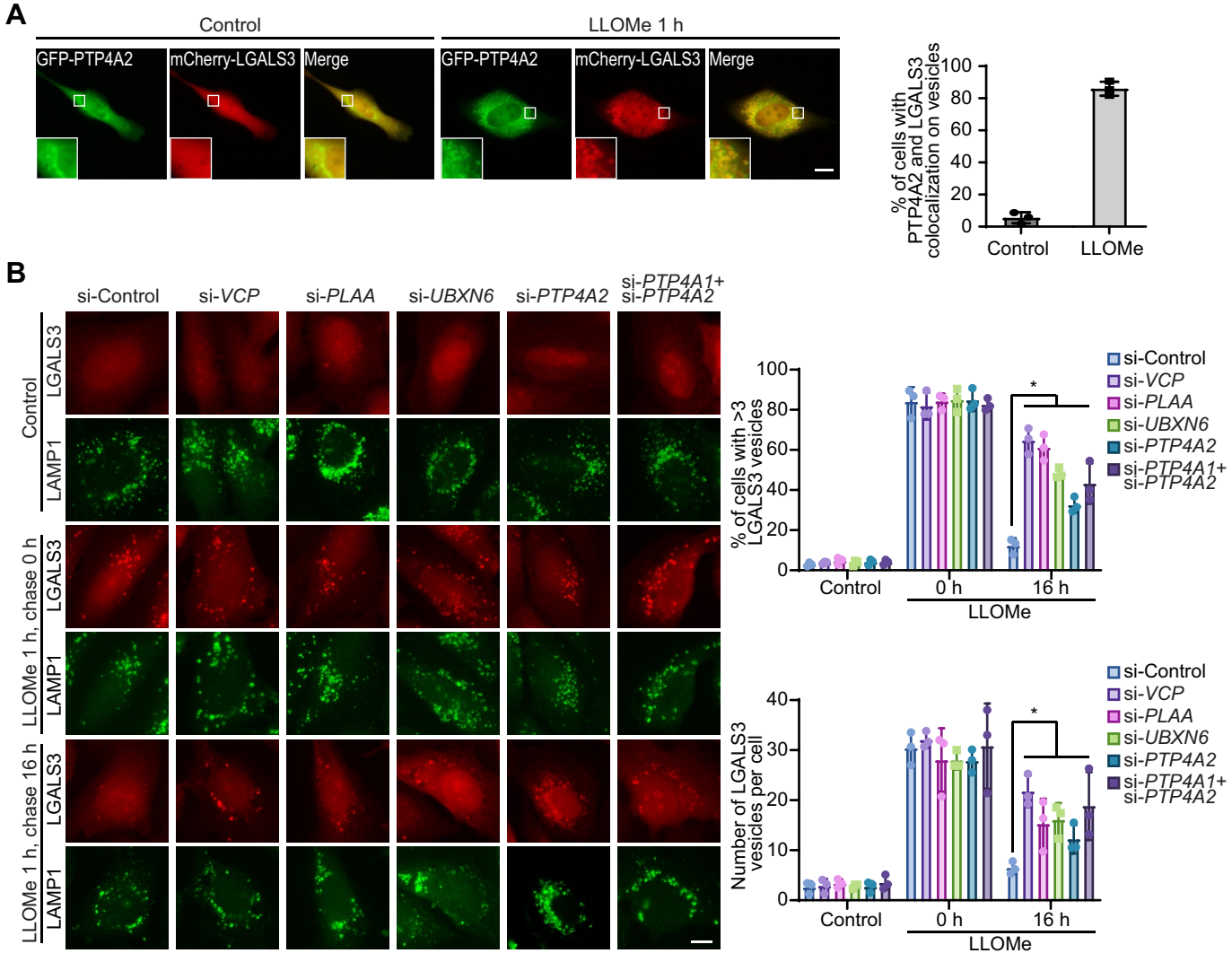

Figure 7. PTP4A2 is required for autophagy-mediated clearance of damaged lysosomes. (**A**). GFP-PTP4A2 and mCherry-LGALS3 were co-expressed in U2OS cells, and then cells were treated with or without LLOMe for 1 h and fixed for imaging at both green and red channel by microscope. The bar graph represents the percentage of cells with PTP4A2 and LGALS3 colocalization on vesicles. Three independent experiments with at least 30 cells in each experiment were used for calculation. (**B**). U2OS cell line stably expressing mCherry-LGALS3 was transfected with siRNAs (set 2) against *VCP, PLAA, UBXN6, PTP4A2* or *PTP4A1* for 72 h. Cells were treated with LLOMe for 1 h, and then recovered for 16 h after washing away of LLOMe. Cells were fixed and stained with LAMP1 antibody. LAMP1 and mCherry-LGALS3 signal were captured by microscope. The bar graphs represent the percentage of cells with more than 3 LGALS3 vesicles and mean number of LGALS3 vesicles per cell. Three independent experiments with at least 30 cells in each experiment were used for calculation. Scale bars: 10 μm.

followed by an unbiased quantitative proteomics approach to identify PTP4A2 neighboring proteins *in situ* in both basal and damaged lysosomes condition. A total of 1689 proteins were identified as PTP4A2-neighboring proteins (Figure 6B and Table S2). Again, VCP was significantly enriched as a PTP4A2 proximal protein in response to lysosomal damage (Figure 6B and 6C). Moreover, 109 plasma membrane proteins and 61 endosomal membrane proteins were identified as expected, while 56 lysosomal membrane proteins were also identified (Figure 6B and 6D). Notably, most of these lysosomal proteins were not enriched upon LLOMe treatment, suggesting PTP4A2's lysosomal localization is not lysosomal damage dependent. Interestingly, a reported K48-ubiquitinated lysophagy target LAMP2 was also found close to PTP4A2 [48], providing biochemical evidence that PTP4A2 is a lysosomal resident protein in the vicinity of ubiquitination substrates upon lysosomal damage (Figure 6D). Gene Ontology (GO) analysis of the PTP4A2 interactomes confirmed the significant enrichment for GO terms linked with lysosomes and autophagy (Figure 6E and 6F).

To explore whether PTP4A2 plays a role in the endolysosomal damage response, we used the lysosomotropic reagent LLOMe, which can specifically and acutely damage late endosomal and lysosomal compartments as visualized by the translocation of cytosolic LGALS3/Gal3 (galectin 3) to the damaged lysosomes (Figure S7A). LLOMe treatment triggered a burst of LGALS3 punctate structures that colocalized with PTP4A2 (Figure 7A), showing recruitment of PTP4A2 to damaged lysosomes. Notably, both PTP4A1 and PTP4A3 also colocalized with LGALS3 puncta upon lysosomal damage (Figure S7B). As expected, knockdown of *VCP, UBXN6* or *PLAA* significantly delay the autophagic clearance of LGALS3-positive vesicles (Figure 7B and S7C) [31]. Likewise, knockdown of *PTP4A2* also increased LGALS3-positive damaged lysosomes after 16 h of LLOMe washout (Figure 7B and S7C), supporting an essential role of PTP4A2 in autophagic clearance of damaged lysosomes. Furthermore, removal of both *PTP4A1* and *PTP4A2* elicited even more damaged lysosome accumulation compared to *PTP4A2* knockdown alone, suggesting a compensatory role of PTP4A1 for loss of PTP4A2 (7B and S7C).

PTP4A2 promotes K48 ubiquitin conjugate removal and autophagosome formation

Lysosomal damage induces extensive protein ubiquitination for recruitment of the autophagy machinery by the LC3-receptor proteins such as SQSTM1/p62 and engulfment of damaged organelle by phagophore membranes [49–51]. Both the K63 and K48 ubiquitin linkages have been detected on damaged lysosomes, but only the K63 chains are responsible for the recruitment of SQSTM1 to the damaged lysosomes for autophagy, while the K48 ubiquitin conjugates need to be removed by the ELDR complex to facilitate LC3 recruitment and autophagosome formation [31]. To determine whether PTP4A2 is required for K48 ubiquitination removal, we assessed the functional relevance of PTP4A2-mediated turnover of K48 conjugates for autophagy. Expression of GFP-PTP4A2 successfully cleared the K48 conjugates on damaged lysosomes, with no significant impact on the K63 chains, suggesting that PTP4A2 promotes specifically the clearance of the K48 linkages (Figure 8A). Further, expression of the catalytically inactive GFP-PTP4A2[DACS] mutant failed to remove K48-positive vesicles and GFP-PTP4A2[DACS] strongly colocalized with K48-decorated lysosomes 8 h after washout (Figure 8A), indicating that PTP4A2 phosphatase activity is required for K48 removal on damaged lysosomes. Additional evidence confirmed that these K48 vesicles are indeed on lysosomes as evidenced by the LAMP1 staining, and expression of HA-PTP4A2 displayed less K48 positive LAMP1 vesicles than HA-PTP4A2[DACS] (Figure S8A). In addition, we also measured K48 removal upon expression of VCP^{Y805F}, a mutant VCP incapable of binding UBXN6 and PLAA. Expression of VCP^{Y805F} but not WT VCP resulted in the accumulation of K48 ubiquitination, but neither of them affected K63-linked ubiquitination (Figure S8B), again suggesting that the PTP4A2-mediated dephosphorylation of VCP at Tyr805 and recruitment of VCP C-terminal cofactors PLAA and UBXN6 are required for K48 removal. Moreover, depletion of *PTP4A2* with siRNA also led to accumulation of K48-positive lysosomes, which is similar to knockdown of ELDR complex components *VCP, PLAA* and *UBXN6* (Figure 8B and S8C). These data suggest that PTP4A2 is required for K48 conjugates removal after lysosomal damage. Strikingly, knockdown of both *PTP4A1* and *PTP4A2* caused marked K48 accumulation even at 2 h after washout (Figure 8B), indicating both PTP4A1 and PTP4A2 are involved in K48 clearance.

To further assess the functional relevance of PTP4A2-mediated turnover of K48 conjugates, we next evaluated if PTP4A2 is required for LC3 recruitment and autophagosome formation around damaged lysosomes. We first inhibited K48 conjugates removal by depletion of *PTP4A2* or both *PTP4A1* and *PTP4A2* and analyzed the accumulation of LC3-negative LGALS3 vesicles 8 h after LLOMe-induced damage. We found that although LC3-decorated membranes accumulated in the vicinity of LGALS3-labeled lysosomes, they failed to colocalize when *PTP4A2* or *PTP4A1* and *PTP4A2* were downregulated, leading to increased number of LC3-negative LGALS3 vesicles (Figure 8C), which is similar to what was observed upon depletion of *VCP* or its C-terminal cofactors *PLAA* and *UBXN6* [31] (Figure 8C). These results suggest that PTP4A2 is also required for the LC3-decorated autophagy fusion with damaged lysosomes. To further investigate whether ELDR component YOD1 deubiquitinase is involved in PTP4A2-mediated K48 removal, we first examined the colocalization of GFP-YOD1 and mCherry-PTP4A2. Indeed, YOD1 translocated to and colocalized with PTP4A2 vesicles upon lysosomal damage (Figure S8D), indicating that PTP4A2 cooperates with YOD1 during lysophagy for K48-linked Ub removal. To further examine the impact of PTP4A2 on YOD1 lysosomal localization, we established *PTP4A2* deleted human osteosarcoma U2OS cells by CRISPR (Figure S8E). VCP is recruited to damaged lysosomes through extensive ubiquitination of lysosomal proteins [31]. As expected, VCP's lysosomal localization upon LLOMe treatment were not affected in *PTP4A2* KO cells (Figure S8F and S8G). Interestingly, although PLAA and UBXN6's lysosomal translocation was not affected by *PTP4A2*

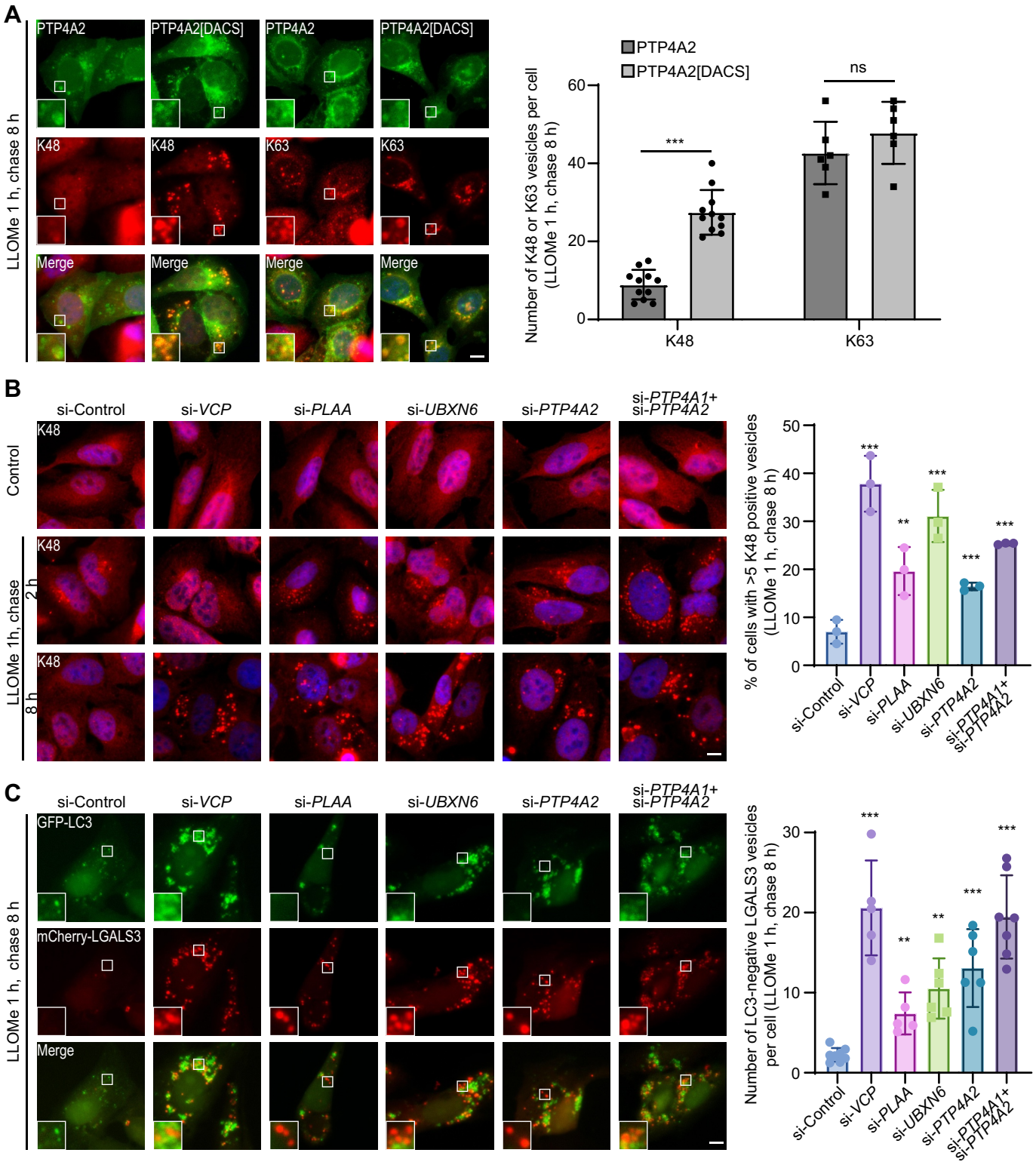

Figure 8. PTP4A2 is required for K48 ubiquitin conjugate removal and autophagosome formation. (**A**). U2OS cells stably expressing GFP-PTP4A2 or GFP-PTP4A2 [DACS] were treated with LLOMe for 1 h, and then cells were recovered for 8 h after removal of LLOMe. Cells were then fixed for IF study with K48-linkage or K63-linkage specific polyubiquitin antibodies. The bar graph represents the mean number of K48- or K63-positive vesicles per cell. At least 6 images with at least 20 cells per image were counted. (**B**). U2OS cell line stably expressing mCherry-LGALS3 was transfected with siRNAs (set 1) against *VCP, PLAA, UBXN6, PTP4A2* or *PTP4A1* for 72 h. Cells were treated with LLOMe for 1 h, and then recovered for 2 h or 8 h after removal of LLOMe. Cells were then fixed for IF study with K48-linkage specific polyubiquitin antibody. The bar graph represents the percentage of cells with at least 5 K48-positive vesicles. (**C**). U2OS cell line stably expressing GFP-LC3 and mCherry-LGALS3 was transfected with siRNAs (set 1) against *VCP, PLAA, UBXN6, PTP4A2* or *PTP4A1* for 72 h. Cells were treated with LLOMe for 1 h, and then recovered for 8 h after removal of LLOMe. Cells were then fixed and GFP and mCherry signals were captured by microscope. The bar graph represents the mean numbers of LC3-negative LGALS3 vesicles per cell. At least 5 images with at least 20 cells per image were counted. Scale bars: 10 μm.

deletion, the recruitment of YOD1 to damaged lysosomes were significantly impaired (Figure S8F and S8G), confirming that PTP4A2-mediated K48 removal is through YOD1. Interestingly, we also found GFP-VCPIP1 (valosin containing protein interacting protein 1), another deubiquitinase with high activity against K48-linked polyUb [52], also translocated to PTP4A2 positive puncta upon lysosomal damage, albeit to a lesser degree than YOD1 (Figure S8D). Importantly, endogenous VCPIP1 also translocated to punctate structures in the presence of LLOMe, which is significantly abolished in *PTP4A2* KO cells (Figure S8F and S8G). Considering VCPIP1 is also the most abundant VCP-binding protein enriched by PTP4A2 overexpression (Table S1), it is possible that VCPIP1 may also be involved in PTP4A2 and VCP mediated lysophagy. Taken together, we conclude that PTP4A2-mediated dephosphorylation of VCP at Tyr805 promotes UBXN6 and PLAA recruitment to VCP, where it may cooperate with YOD1 [31] or other deubiquitinases, such as VCPIP1, to remove the K48 conjugates on damaged lysosomes to enable autophagosome formation and clearance of the damaged lysosomes.

PTP4A2 is required for recovery from acute kidney injury in mice

Autophagy is required for protection of acute kidney injury (AKI) by sequestering damaged lysosomes [23,53]. To assess the physiological function of PTP4A2 in driving clearance of damaged lysosomes by autophagy, we utilized a rhabdomyolysis induced AKI mouse model. Rhabdomyolysis, characterized by injury to skeletal muscle fibers, can induce AKI as a severe complication [54]. We found PTP4A2 is highly expressed in the epithelium of renal proximal and distal tubules (Figure 9A). To investigate the pathophysiological importance of PTP4A2 in rhabdomyolysis induced AKI, we compared the recovery efficiency after glycerol-induced AKI in WT and *ptp4a2* KO mice (Figure 9B). HE staining demonstrated that *ptp4a2*$^{-/-}$ mice exhibited delayed recovery from AKI as evidenced by the persistent loss of brush border, vacuolization, tubular dilation, and cast formation in renal tubules, while all WT mice recovered by day 9 (Figure 9C). We further evaluated the kidney function by determining the serum urea nitrogen. On AKI day 3, both WT and *ptp4a2*$^{-/-}$ mice contained significantly elevated serum urea nitrogen, which returned to the normal level on AKI day 9 for the WT but not the *ptp4a2*$^{-/-}$ mice (Figure 9D), further confirming the delayed recovery from AKI in *ptp4a2*$^{-/-}$ mice.

To further evaluate if the delayed recovery from AKI in *ptp4a2* KO mice is due to the failure of autophagy-mediated clearance of damaged lysosomes, we first performed immunohistochemistry (IHC) staining with LAMP1 (a lysosome marker) and LGALS3 (a damaged lysosome marker) to show lysosomal damage. LAMP1 staining revealed enlarged lysosomes in both WT and *ptp4a2*$^{-/-}$ kidney at AKI day 3, which was completely diminished only in WT mice at AKI day 9 (Figure S9A). LGALS3 staining showed that on day 3 of the AKI experiment, renal tubules have accumulated lysosomal damage, which were eliminated on day 9 in WT mice, but not in *Ptp4a2* deficient mice, suggesting that *Ptp4a2* deletion causes an extended lysosomal damage in renal tubules (Figure 9E). Electron microscopy analysis revealed accumulation of damaged lysosomes in kidneys from both WT and *ptp4a2*$^{-/-}$ on day 3, which persisted only in *ptp4a2*$^{-/-}$ mice on day 9 (Figure S9B). We then performed LC3 (an autophagosome marker) and polyUb-K48 (ELDR substrates) staining. Interestingly, LC3 staining indicated that *Ptp4a2* deletion did not affect autophagosome initiation because autophagy could still be induced by the lysosomal damage on day 3 and disappear on day 9 in both WT and *ptp4a2* KO mice (Figure 9F). Furthermore, rhabdomyolysis-mediated AKI prompted an immediate accumulation of K48 ubiquitination in renal tubules, which was eliminated on day 9 of AKI experiment in WT mice, whereas deletion of *Ptp4a2* caused a prolonged accumulation of K48 ubiquitination even on day 9 (Figure 9G). Given the newly established role of PTP4A2-mediated dephosphorylation of VCP at Tyr805 in ELDR complex assembly (Figure 4 and Table S1), we next examined VCP Tyr805 phosphorylation and its cofactor recruitment in kidney samples. As expected, VCP Tyr805 phosphorylation was significant reduced on day 3 after AKI and recovered on day 9 in WT mice, as evidenced by both 4G10 and p-VCP (Tyr805) antibody (Figure 9H). Accordingly, UBXN6 and PLAA association with VCP were clearly enhanced on day 3, and then reduced to basal level on day 9 (Figure 9H). In contrast, VCP Tyr805 phosphorylation as well as PLAA and UBXN6 recruitment did not change in *ptp4a2*$^{-/-}$ mice (Figure 9H). Since transcription factor EB (TFEB) activation is essential for lysosomal damage response to kidney injury [55], we then measured the TFEB activation in the kidney samples. Inactive TFEB is phosphorylated by mTOR and sequestered in the cytosol, whereas dephosphorylation and nucleus translocation will active TFEB to promote autophagy and lysosomal biogenesis [56,57]. IHC study showed that nuclear translocation of TFEB occurred on day 9 of WT but not in *ptp4a2*$^{-/-}$ kidney (Figure S9C). Western blot further confirmed TFEB down-shifted (due to dephosphorylation) only in WT kidney samples on day 9, which was not observed in *ptp4a2*$^{-/-}$ mouse kidney (Figure S9D), indicating that the impaired damaged kidney repair in *Ptp4a2* deletion is at least partially due to failure of TFEB activation. Future studies are needed to determine if TFEB activation is dependent on PTP4A2 mediated VCP dephosphorylation. Altogether, these data strongly support that PTP4A2 promotes K48 conjugates removal *in vivo* through dephosphorylating VCP at Tyr805 and augmenting ELDR complex formation, which facilitates autophagy-mediated clearance of damaged lysosomes in rhabdomyolysis induced AKI.

Discussion

The PTP4A phosphatases are novel anti-cancer targets due to their aberrant expression in advanced tumors [2–4,14]. However, the underlying mechanism(s) of action for the PTP4As are not completely understood. Unraveling the molecular basis of PTP4As in normal and disease biology is essential for the development of PTP4A-based therapeutics. Although a non-catalytic role for the PTP4As in modulating

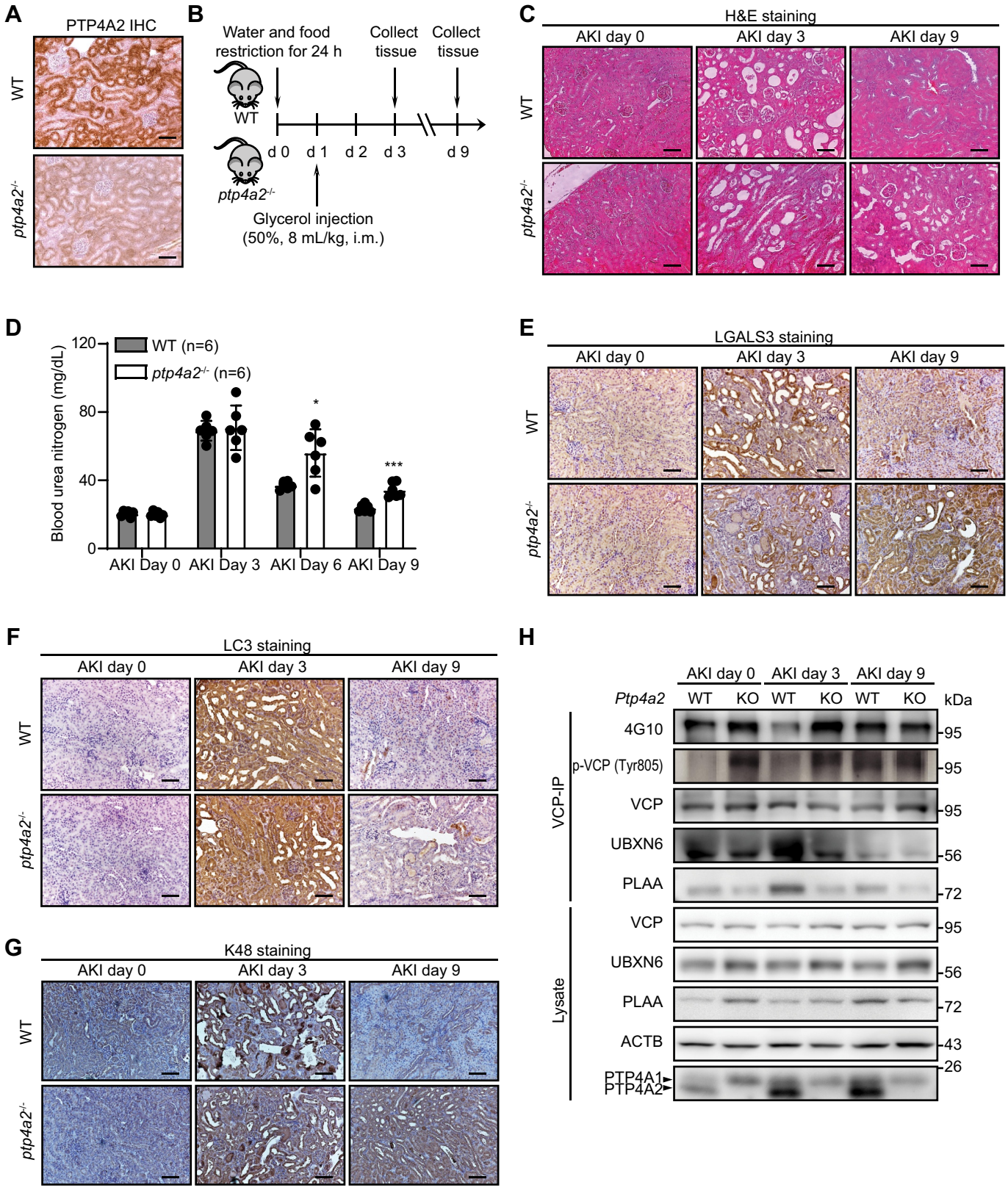

Figure 9. *Ptp4a2* deletion delayed the recovery of glycerol-injection induced acute kidney injury. (**A**). Kidneys were isolated from WT and *ptp4a2* KO mice, and IHC was performed with PTP4A2 antibody. Scale bars: 100 μm. (**B**). Illustration of the experimental design for glycerol-injection mediated acute kidney injury (AKI) model. (**C**). Kidneys were collected at 3 days or 9 days after AKI from WT and *ptp4a2* KO mice, and H&E staining was performed. Scale bars: 100 μm. (**D**). Blood was collected at 3 days, 6 days, or 9 days after AKI from WT (n = 6) and *ptp4a2* KO (n = 6) mice, and blood urea nitrogen was measured as indicator of kidney injury. (**E – G**). Kidneys were collected at 3 days or 9 days after AKI from WT and *ptp4a2*KO mice, and IHC was performed with LGALS3 (**E**), LC3 (**F**) and K48-linage specific polyubiquitin (**G**) antibodies, respectively. Scale bars: 100 μm. (**H**). Kidneys were collected at 3 days or 9 days after AKI from WT and *ptp4a2* KO mice, and VCP-IP was performed from kidney lysates. The lysate and bound proteins were blotted with phosphotyrosine (4G10), p-VCP (Tyr805) specific, VCP, PLAA, UBXN6, ACTB and PTP4A1 and PTP4A2 antibodies.

intracellular Mg^{2+} concentration has been described [14], the phosphatase activity is required for many of the PTP4A functionalities [18,58,59]. Consequently, identification and characterization of physiological substrates for the PTP4As will be key to understanding many of their actions in cellular physiology and oncogenic development. We previously established PTEN as a substrate for PTP4As and showed that PTP4A2 promotes tumorigenesis by dephosphorylating PTEN at Tyr336, thereby augmenting the NEDD4-mediated PTEN ubiquitination and proteasomal degradation [18]. Here we identify VCP (p-Tyr805) as a substrate for PTP4A2 using substrate trapping, mass spectrometry, and rigorous biochemical analyses. We further demonstrate that, through dephosphorylation of VCP at Tyr805, PTP4A2 functions as a crucial regulator of VCP to promote lysophagy. These findings offer a new mechanism whereby PTP4A2 normally plays a cytoprotective and homeostatic role and can support cancer progression when upregulated.

VCP regulates cellular homeostasis via its capacity to coordinate both the ubiquitin-proteasome mediated protein degradation and autophagy for macromolecule quality control and turnover [26,27]. Changes in VCP expression or activity have been implicated in the development of cancer [43,60,61] and neurodegenerative disorders [62,63]. Although better known for its ability to direct ubiquitinated proteins to the proteasome [28,41,64], VCP is also a critical regulator of autophagy [29–31,65-67], a cellular housekeeping process that gets rid of large protein aggregates and damaged organelles through the lysosome [21]. However, the biochemical mechanism by which VCP participates in the autophagy process has been enigmatic. Recent work from Hemmo Meyer's group uncovered an endo-lysosomal damage response (ELDR) complex through which VCP cooperates with its specific cofactors PLAA, UBXN6 and YOD1 to maintain lysosomal homeostasis through autophagy [31]. However, how the ELDR complex is regulated remains unclear. Moreover, the biological significance of the penultimate and conserved Tyr805 phosphorylation in VCP has not been established.

To perform its various cellular duties, VCP engages with a large number of enzymes and adaptor proteins through its N-terminal domain and C-terminal tail [68]. The PUB domain of UBXN6 and PUL domain of PLAA are known to bind the C-terminal tail of VCP [68]. Structural studies have shown that the VCP-PUB or VCP-PUL complex is primarily maintained by the hydrophobic Leu804 as well as the aromatic side chain of the penultimate Tyr805 of VCP, which inserts into a hydrophobic pocket in the PUB or PUL domain [68]. Phosphorylation of Tyr805 completely abolishes the interaction between VCP and the PUB or PUL domain [37,40,69]. Since Tyr805 of VCP is highly phosphorylated inside the cells [70], we surmised that its dephosphorylation may serve as a control mechanism for the recruitment of VCP C-terminal cofactors. We demonstrate here that PTP4A2 promotes the association of VCP with UBXN6 and PLAA, which are components of the ELDR complex responsible for autophagy mediated clearance of damaged lysosomes, by catalyzing the removal of the phosphate from the penultimate and conserved Tyr805 in VCP.

In addition to the VCP C-terminal cofactors PLAA and UBXN6, the N-terminal cofactor YOD1 deubiquitinase is also involved in the lysophagy pathway for K48 ubiquitin conjugate removal, thereby facilitating the autophagosome fusion to the damaged lysosome [31]. Although we were unable to detect YOD1 in the VCP complexes either by IP or mass spectrometry analysis (Figure 4 and Table S1), we confirmed that YOD1 is involved in PTP4A2-mediated K48 removal. Interestingly, we also found that VCPIP1, a deubiquitinase with high activity against K48-linked polyUb [52], significantly increased its interaction with VCP upon PTP4A2 expression (Table S1). It has been reported that VCPIP1 does not localize to damaged lysosomes when tagged with GFP on either N or C terminus, but knockdown of

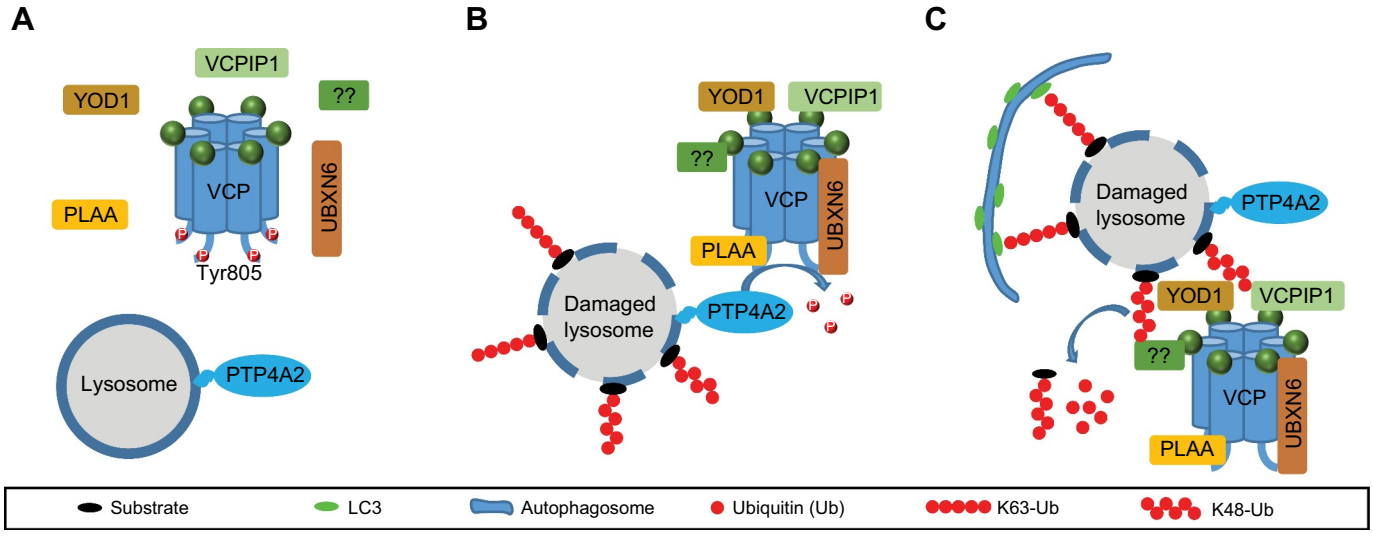

Figure 10. A working model for PTP4A2-mediated VCP p-Tyr805 dephosphorylation, ELDR complex formation, and damaged lysosome clearance. (**A**). VCP is localized in the cytosol in the resting state, while PTP4A2 is a lysosomal resident protein. (**B**). Lysosomal damage triggers extensive ubiquitination of lysosomal proteins, which recruit VCP from the cytosol to damaged lysosomes, where PTP4A2 dephosphorylates the lysosomal translocated VCP to facilitate the ELDR complex assembly on the damaged lysosomes (**C**). The ELDR complex promotes K48 conjugates removal, leading to successful autophagosome formation and damaged lysosome clearance.

endogenous *VCPIP1* significantly delayed damaged lysosome clearance, indicating that VCPIP1 is a possible alternative deubiquitinase for the ELDR complex [31]. We found that GFP-tagged VCPIP1 can translocate to PTP4A2-positive vesicles upon lysosomal damage. Most importantly, endogenous VCPIP1 also formed punctate structure in response to LLOMe treatment, which was abolished upon VCP or PTP4A2 knockdown. Further investigation is needed to determine the functional requirement of different deubiquitinases in lysophagy.

We have established a functional linkage between PTP4A2 and autophagy (Figure 10). It has been previously shown that PTP4A2 is localized on the plasma membrane and endosomal compartments through its C-terminal CAAX motif prenylation [8,44–47]. In this study, we found that PTP4A2 is localized on lysosomes as evidenced by its colocalization with lysosomal marker LAMP1 in both basal and lysosome damage conditions (Figure 6A and 10A). VCP is known to be localized in the cytosol in the resting state (Figure 10A). Lysosomal damage will trigger extensive ubiquitination of lysosomal proteins, which recruit VCP from cytosol to damaged lysosomes [31]. Our results suggest that PTP4A2 is a lysosomal resident protein and upon lysosomal damage PTP4A2 can dephosphorylate the lysosomal translocated VCP at Tyr805 to facilitate the ELDR complex assembly on the damaged lysosomes (Figure 10B) in order to prepare for the efficient clearance of the damaged lysosomes by the ELDR complex (Figure 10C). Cancers are characterized by a high metabolic demand and increased levels of oxidative stress, which often cause lysosomal membrane permeabilization [22]. As a final destination for autophagy, lysosome homeostasis is extremely important for the survival of cancer cells due to the increased metabolic and biosynthetic demands caused by uncontrolled proliferation [21]. Therefore, cancer cells often hijack lysophagy to survive such stresses to ensure lysosomal quality control. Autophagy activity also increases in late-stage cancer or metastasis through establishing the pre-metastatic niche, promoting tumor cell survival, and escaping from immune surveillance to ultimately grow out an overt metastasis [71,72]. Indeed, pharmacologically inhibition of autophagy may represent an effective therapeutic strategy for advanced cancer [73].

The ability of PTP4A2 to dephosphorylate VCP may explain the oncogenic potential of PTP4A2 in driving efficient lysophagy to support lysosomal hemostasis and survival in cancer cells. Therefore, small molecular inhibitors that target the PTP4A family members could be used to block lysophagy and lysosomal homeostasis, and this can serve as a novel cancer therapeutic approach for treating autophagy-addicted cancers, in addition to existing VCP and autophagy inhibition strategies.

This study reveals a novel regulatory role of PTP4A2 in promoting the ELDR complex assembly and lysophagy, but the detailed mechanism of how the C-terminal cofactors UBXN6 and PLAA work together with VCP in lysophagy requires further study. In addition to PLAA and UBXN6, PTP4A2 mediated VCP Tyr805 dephosphorylation may also enhance the association of VCP with two other PUB domain-containing proteins NGLY1/PNGase, a peptide N-glycanase involved in the deglycosylation of misfolded glycoproteins [74], and RNF31/HOIP (ring finger protein 31), the catalytic subunit of the E3 ubiquitin ligase LUBAC, which catalyzes the assembly of linear ubiquitin chains [75]. Further investigation is required to ascertain whether PTP4A2 regulates VCP binding to NGLY1/PNGase and RNF31/HOIP. Moreover, UBXN6 employs a unique bipartite binding mode where its PUB domain binds the VCP C terminus and its VIM motif interacts with the N-terminal domain of VCP [39], which may restrict the conformational flexibility of VCP. Therefore, PTP4A2-mediated UBXN6-VCP association could also trigger an overall conformational change of VCP, which may affect VCP N-terminal domain cofactor binding. Indeed, we found PTP4A2 expression not only changes VCP C-terminal cofactor association, but also alters the overall N-terminal domain cofactor binding profile (Figure 4E and Table S1). Future studies will determine the functional significance of the additional changes to VCP cofactor binding profile affected by PTP4A2, especially the interaction of VCPIP1 and VCP in lysophagy.

In summary, we have identified VCP (p-Tyr805) as a physiological substrate of PTP4A2. Dephosphorylation of VCP at Tyr805 by PTP4A2 promotes its association with the C-terminal cofactors PLAA and UBXN6, resulting in the formation of the ELDR complex. PTP4A2 stimulates the ELDR complex-mediated removal of K48-linked ubiquitin conjugates on damaged lysosomes for autophagosome formation and clearance of lysosomal damage. Deletion of *Ptp4a2* in mice results in delayed recovery from glycerol-induced AKI due to impaired function of the ELDR complex on damaged lysosomes. Our findings not only for the first time establish a functional linkage of PTP4A2 to the endo-lysosomal homeostasis and autophagy, but also implicate potential disease connections of hyperactivation of PTP4A2 in cancer and impairment of PTP4A2 activity in lysosomal damage induced diseases, such as rhabdomyolysis-induced kidney injury and myodegenerative and neurodegenerative disorders.

Materials and methods

Animals

The *ptp4a2* KO mice ($ptp4a2^{-/-}$) used in this study was described previously [16]. For acute kidney injury mouse model, experiment animals were deprived of water and food for 24 h and then injected with glycerol (50%, 8 mL/kg) deeply into the muscle of hind-legs to induce necrosis of muscle cells. Two days, five days and eight days after injection, serums were collected for blood urea nitrogen (BUN) analysis according to manufacturer's recommendations (ThermoFisher Scientific, EIABUN), while kidneys were collected for either western blot or histology analysis. All mice were maintained in either Indiana University School of Medicine animal facility or Purdue University animal facility according to the respective Institutional Animal Care and Use Committee (IACUC) -approved protocols, and kept in Thorensten units with filtered germ-free air.

Cell culture and treatment

MEF cells were isolated from *Ptp4a2*-deficient mice [18]. HEK293 (ATCC, CRL-1573), H1299 (ATCC, CRL-5803), MCF7 (ATCC, HTB-22), HCT116 (ATCC, CCL-247), U2OS (ATCC, HTB-96), GC-1 (ATCC, CRL-2053), HeLa (ATCC, CCL-2) and Ub^{G76V}-GFP-expressing HeLa cells, a gift from Dr. Eli Chapman (University of Arizona) [42] were grown in DMEM (Corning Cellgro, 10–013-CV), while Kasumi-1 (ATCC, CRL-2724), K562 (ATCC, CCL-243), U937 (ATCC, CRL-1593.2) and HL-60 (ATCC, CCL-240) cells were grown in RPMI 1640 (Corning Cellgro, 10–040-CV) supplemented with 10% fetal bovine serum (Gibco, 26,400,044), penicillin (50 units/mL), and streptomycin (50 μg/mL) (Corning, MT30002CI) in a 37°C incubator containing 5% CO_2. Cells were seeded at 40–80% confluence in antibiotic-free medium and grown overnight. Transfection was performed using PEI (Polysciences, 23,966–2), Lipofectamine 2000 (Invitrogen, 11,668,019) or RNAiMAX (Invitrogen, 13,778,075) according to the manufacturer's recommendations. Two sets of siRNAs against *VCP, PLAA, UBXN6, PTP4A2* and *PTP4A1* were purchased from Integrated DNA Technologies (set 1) and Santa Cruz Biotechnology (set 2), respectively. Cells were treated with NMS-873 (Sigma-Aldrich, SML1128) or LLOMe (Sigma-Aldrich, L7393) as indicated in the text.

Antibodies

Anti-PTP4A1 and PTP4A2 antibody was a gift from Dr. Zeng's lab (National University of Singapore) [76], anti-p-VCP (Tyr805) antibody was generated by Biomatik using VCP (p-Tyr805) peptide CSVYTEDNDDDLpYG. Anti-phosphotyrosine (4G10; Millipore, 05–321), anti-ubiquitin, Lys48-specific, clone Apu2 (Millipore, 05–1307), anti-ubiquitin, Lys63-specific, clone Apu3 (Millipore, 05–1308), anti-phosphotyrosine (PY20; BD biosciences, 610,000), anti-VCP (ThermoFisher Scientific, MA3-004), anti-GFP (D5.1; Cell Signaling Technology, 2956), anti-PLAA (Santa Cruz Biotechnology, sc-390,454), anti-LGALS3/galectin-3 (Santa Cruz Biotechnology, sc-32,790), anti-ACTB/actin (Santa Cruz Biotechnology, sc-47,778), anti-HA (Santa Cruz Biotechnology, sc-7392), anti-PLAA (Abcam, ab133589), anti-UBXN6/UBXD1 (Abcam, ab103651), anti-Flag, M2 (Sigma-Aldrich, F1804), anti-LC3B (Sigma-Aldrich, L7543), anti-Flag affinity gel (Bimake, B23102), anti-LAMP1 (Santa Cruz Biotechnology, sc-20,011), anti-VCPIP1 (Santa Cruz Biotechnology, sc-515,291), anti-TFEB (ThermoFisher Scientific, A303-673A; for western blot), anti-TFEB (ThermoFisher Scientific, PA1-31,552; for IHC), anti-Biotin (Santa Cruz Biotechnology, sc-57,636) are commercially available.

Immunoprecipitation and immunoblotting

For Immunoprecipitation, cells were lysed in the lysis buffer (20 mM Tris, pH 7.5, 150 mM NaCl, 10% glycerol, 1% Triton X-100 [Fisher Scientific, BP151-100]) supplied with phosphatase inhibitor (Bimake, B15002) and protease inhibitor mixture (Roche Applied Science, 04693132001) and cleared by centrifugation at 21,000 g, 10 min. Antibody and protein A/G beads (Santa Cruz Biotechnology, sc-2003) were then added to cell lysates and incubated at 4°C for 3 h to overnight followed by extensively washing with the lysis buffer. Proteins on the resins were eluted with SDS sample buffer and then subjected to analysis by SDS-PAGE followed by western blot with appropriated antibodies. For immunoblotting, tissues or cultured cells were lysed with ice cold lysis buffer. Equal amounts of protein were resolved by SDS-PAGE, transferred to nitrocellulose membrane and subjected to immunoblotting.

Substrate-trapping assay

For substrate trapping with recombinant protein by GST affinity isolation, cells (1×10^9) were treated with 1 mM pervanadate (ThermoFisher Scientific, 207,991,000) for 30 min and collected by centrifugation at 21,000 g, 10 min. The cell pellet was lysed with 3 mL lysis buffer (20 mM Tris, pH 7.5, 100 mM NaCl, 1% Triton X-100, 10% glycerol, 5 mM iodoacetic acid, 1 mM orthovanadate, protease inhibitors). Dithiothreitol (10 mM) was added to the lysate and incubated for 15 min on ice to inactivate any unreacted iodoacetic acid and pervanadate. Supernatant was collected by centrifugation at 17,000 g for 15 min. Wild-type PTP4A2 or substrate-trapping mutant $PTP4A2^{D69A,C101S}$ (PTP4A2[DACS]) were fused to GST or His-tag [77]. GST, GST-PTP4A2, or GST-PTP4A2[DACS], or His-tagged PTP4A2 or His-tagged $PTP4A2^{C101S}$ (25 μg) was coupled to GST beads (Sigma-Aldrich, GE17-0756-05) or Ni-NTA beads (Qiagen, 30,230), respectively, in lysis buffer, and incubated at 4°C for 1 h. Cell lysates were incubated with PTP4A2 proteins conjugated to beads at 4°C for 2 h. For substrate trapping inside the cell by IP, cells in 15-cm dishes were transfected with Flag-PTP4A2 or Flag-PTP4A2[DACS] for 24–48 h. The transfected cells were treated with 300 μM pervanadate for 30 min, the medium was replaced with fresh medium for another 30 min, and the cells were collected by centrifugation. The cell pellet was lysed with 1 mL lysis buffer on ice for 1 min and then spun at 17,000 g at 4°C for 30 min, and the supernatant was transferred to a fresh tube and Flag agarose beads added and incubated at 4°C for 3 h. Beads were collected by centrifugation at 3,600 g for 1 min and the supernatant was removed. Beads were washed three times with 1.5 mL lysis buffer. Bound proteins were resuspended in 50 μL Laemmli sample buffer and boiled for 5 min, and the samples were resolved by SDS-PAGE.

APEX2-PTP4A2 proximity labeling

PTP4A2 was sub-cloned into Flag-APEX2-C vector (Addgene, 128,146; deposited by Ken-Ichi Takemaru). HEK293 cells stably expressing APEX2-PTP4A2 was established by transient transfection and selection in growth media containing 1 μg/mL puromycin. Cells were cultured in 90% confluent and then treated with or without 250 μM LLOMe for 3 h. The biotinylation protocol was performed as previously described [78]. For enrichment of biotinylated proteins, cells were lysed

in lysis buffer, and NeutrAvidin agarose (ThermoFisher Scientific, 29,200) was used for protein purification.

On-bead digestion

Samples were reduced and alkylated with 10 mM tris-(2-carboxyethyl)phosphine (Sigma-Aldrich, C4706) and 40 mM chloroacetamide (Sigma-Aldrich, C0267) in 50 mM Tris-HCl, pH 8.5 at 95°C for 5 min. The reduced and alkylated proteins were diluted by 5-fold with 50 mM triethylammonium bicarbonate (TEAB; Sigma-Aldrich, 18,597) buffer. Trypsin (500 ng) was added to each sample for overnight digestion at 37°C. The trypsin digestion was stopped by adding trifluoroacetic acid (TFA; Sigma-Aldrich, T6508) to a final concentration of 0.5%. The tryptic peptides were desalted by homemade stage tip with styrene divinyl benzene (SDB-XC) membrane (3 M, E520).

Dimethyl labeling

The desalted peptides were dissolved in 100 µl of 100 mM TEAB and were mixed with 4 µL of 4% heavy ($^{13}CD_2O$; Sigma-Aldrich, 596,388) for HA-PTP4A2-overexpressing H1299, WT MEF cells or LLOMe treated APEX2-PTP4A2 expressing HEK293 cells or 4% light ($^{12}CH_2O$; Sigma-Aldrich, 606,758) for control H1299, *ptp4a2* KO MEF cells or untreated APEX2-PTP4A2-expressing HEK293 cells, and then 4 µL of freshly prepared 600 mM sodium cyanoborohydride (Sigma-Aldrich, 156,159) [79]. The mixture was agitated for 1 h at room temperature. The reaction was quenched by adding ice-cold 16 µL of 1% ammonium hydroxide and agitated the mixture for 1 min. Heavy and light dimethyl labeling peptides were mixed after the labeled peptides were acidified with 20 µL of 10% formic acid and then desalted by homemade stage tip with SDB-XC membrane. After elution, 5% of the collected sample were separated for total proteomics analysis. The remaining sample was used for IMAC-Fe phosphopeptides enrichment.

LC-MS/MS

The enriched phosphopeptides were dissolved in 5 µL of 0.3% formic acid (FA) with 3% ACN and injected 4 µL into an Easy-nLC 1000 (ThermoFisher Scientific, LC120). Peptides were separated on a 45-cm in-house packed column (360 µm o.d. × 75 µm i.d.) containing C18 resin (2.2 µm, 100 Å; Michrom Bioresources, 9,996,610,000) with a 30-cm column heater (Analytical Sales and Services) set at 50°C. The mobile phase buffer consisted of 0.1% FA in ultra-pure water (buffer A) with an eluting buffer of 0.1% FA in 80% ACN (buffer B) run over a linear 60 min gradient of 5%–30% buffer B at a flow rate of 250 nL/min. The Easy-nLC 1000 was coupled online with a LTQ-Orbitrap Velos Pro mass spectrometer (ThermoFisher Scientific). The mass spectrometer was operated in the data-dependent mode, in which a full MS scan (from m/z 350–1500 with the resolution of 30,000) was followed by the 10 most intense ions being subjected to collision-induced dissociation (CID) fragmentation (normalized collision energy – 35%; automatic gain control target – 3E4; max injection time – 100 ms; isolation window – 3 m/z; 60s dynamic exclusion).

Data processing and analysis

The raw files were searched against the *Homo sapiens* or *mus musculus* database with no redundant entries (Uniprot FASTA file released Jan 2015) using the MaxQuant software (version 1.5.5.1) with a 1% FDR cutoff at protein and peptide. MS1 precursor mass tolerance was set at 20 ppm, and MS2 tolerance was set at 0.6 Da. Search criteria included a static carbamidomethylation of cysteines (+57.0214 Da) and variable modifications of oxidation (+15.9949 Da) on methionine residues, acetylation (+42.011 Da) at N terminus of proteins, and phosphorylation (+79.996 Da) on serine, threonine, and tyrosine residues for the identification of phosphorylation sites. A site localization probability of 0.75 was used as the cutoff for localization of phosphosites. The search was performed with full tryptic digestion and allowed a maximum of two missed cleavages on the peptides analyzed from the sequence database. Dimethyl-labeling quantitation was performed by setting the multiplicity as 2, and the match between runs function was enabled with a match time window of 1.0 min.

Generation of semisynthetic VCP (p-Tyr805) protein

The protein ligation is performed with IMPACT (Intein Mediated Purification with an Affinity Chitin-binding Tag) system (New England Biolabs, E6901S). Specifically, the pTXB1 plasmid containing VCP (aa 1-793)-MxeIntein-CBD fusion protein was expressed in *E. coli* BL21 (DE3), induced by 0.4 mM IPTG (Fisher Scientific, BP1755-1) at 20°C. Cells were pelleted and lysed by sonication in a lysis buffer (20 mM HEPES, pH 7.6, 150 mM NaCl, 1 mM EDTA). The clarified lysate with cell debris removed was loaded to chitin resin (New England Biolabs, S6651S). The resin was washed with washing buffer (20 mM HEPES, pH 7.6, 150 mM NaCl), and incubated in cleavage buffer (20 mM HEPES, pH 7.6, 150 mM NaCl, 100 mM MESNA [Sigma-Aldrich, 1,392,807], 1 mM EDTA) overnight at 4°C. Cleaved VCP thioester protein was eluted from the resin and concentrated by ultrafiltration using an Amicon filter (Millipore, UFC503008). To generate semisynthetic VCP (p-Tyr805) protein, VCP thioester reacted with chemically synthesized phosphorylated peptide ($_{794}$CVYTEDNDDDLpYG$_{806}$) in the ligation buffer (20 mM HEPES pH 7.6, 150 mM NaCl, 1 mM EDTA, 100 mM MESNA) at room temperature for 18 h. The ligation reaction was assessed by standard and Phos-tag SDS-PAGE (Wako Chemicals, NC1051662) with Coomassie Brilliant Blue staining and immunoblot with an antibody against p-VCP (Tyr805).

Histology

Tissues were fixed in 4% paraformaldehyde (ThermoFisher Scientific, 28,908) overnight at 4°C, embedded in paraffin, serially sectioned (7 µm), and stained with H&E according

to standard methods. For immunohistochemistry, deparaffined and hydrated sections were subjected to antigen retrieval by boiling in 10 mM sodium citrate for 20 min. Sections were then incubated with diluted antibodies (1:50–1:400) at 4°C overnight. Signals were detected by VECTASTAIN Elite ABC kit and developed using DAB substrate (Vector laboratory, SK-4100). Images were captured with a Nikon Inverted Microscope Eclipse Ti-S (Nikon Instruments).

Imaging and immunofluorescence

pIRESpuro2-UBXD1-mCherry (Addgene, 31,835; deposited by Hemmo Meyer), pEGFP-PLAA (Addgene, 85,669; deposited by Hemmo Meyer), LAMP1-RFP (Addgene, 1817; deposited by Walther Mothes), pmCherry-Gal3 (Addgene, 85,662; deposited by Hemmo Meyer), RFP-RAB5 (Addgene, 14,437; deposited by Ari Helenius), EGFP-LC3 (Addgene, 11,546; deposited by Karla Kirkegaard) were used to examine the cellular localization of corresponding genes. Cells were cultured directly on glass coverslips in 12- or 24-well plates. After experiments, cells were fixed with 4% paraformaldehyde in phosphate-buffered saline (PBS; Corning, 20–031-CV) for 15 min at room temperature, permeabilized with 0.2% Triton X-100 in PBS for 10 min, and blocked with BSA (Sigma-Aldrich, A2153). For immunofluorescence, appropriate antibodies were applied overnight at 4°C, followed by wash and 1 h incubation with appropriate secondary antibody. DNA staining (0.5 μg of Hoechst no. 33,258/ml; Sigma-Aldrich, 94,403) was used to identify cell nuclei. After washing with PBS, the coverslips were mounted with anti-fade mounting solution. Images were obtained with a Nikon Inverted Microscope Eclipse Ti-S (Nikon Instruments).

Kinetic measurements for VCP (p-Tyr805) peptide

Initial rate measurements for the enzyme-catalyzed hydrolysis of the substrates were performed as described previously [80]. The VCP (p-Tyr805) peptide Cys-SVYTEDNDDDL(pY)G kinetic assays were carried out at 37°C in a pH 7.0 buffer of 50 mM 3,3-dimethylglutarate (Sigma-Aldrich, D4379), containing 10 mM DTT and 1 mM EDTA, with an ionic strength of 0.15 M, adjusted by addition of NaCl. Assay mixtures of 100 μL in total volume were set up in a 96-well polystyrene plate. A maximum substrate concentration of 1.3 mM of VCP (p-Tyr805) peptide was used to determine the k_{cat} and K_M values. Reactions were started by the addition of PTP4A2 (2 μM). The reaction was carried out at 37°C for 4 h. The reaction was quenched using 100 μL of Biomol Green (Enzo Life Sciences, BML-AK111-0250). After 20 min incubation at room temperature, the absorbance at 620 nm was read using a plate reader. The amount of inorganic phosphate released was calculated using a phosphate standard curve. The data were directly fit to the Michaelis-Menten equation and steady-state kinetic parameters were determined.

Kinetic measurements for VCP (p-Tyr805) protein

First-order rate measurements for the enzyme-catalyzed hydrolysis of the substrates were performed as described previously [18,81].The assay mixtures of 15 μL in total volume were set up with 5 μM of the VCP (p-Tyr805) protein and 1 μM of PTP4A2 and the dephosphorylation was performed over a time course. The VCP (p-Tyr805) protein dephosphorylation over time was analyzed using the specific p-VCP (Tyr805) antibody by western blot and normalized to total VCP concentration. The normalized VCP (p-Tyr805) protein intensities were used to plot a first-order rate plot. The k_{cat}/K_M value was calculated by dividing the first-order rate constant by the enzyme concentration.

Electron microscopy imaging

Kidneys were perfused, fixed (0.1 M sodium cacodylate [Sigma-Aldrich, 20,840] with 4% paraformaldehyde, 0.1% electron microscopy grade glutaraldehyde [Sigma-Aldrich, G5882], pH 7.3–7.4) and desired regions were cut into small pieces (0.5–1.0 mm cube-shaped). Tissue samples were further fixed in 2.5% glutaraldehyde in 0.1 M cacodylate buffer overnight at 4°C and then washed 3 times for 5 min each with 0.1 M sodium cacodylate buffer. After washing, tissue samples were further fixed with 1% OsO_4 (Sigma-Aldrich, 201,030) and 0.8% FeCN (Sigma-Aldrich, P3289) for 1 h, then washed 3 times for 5 min each with water. Samples were stained with 2% uranyl acetate in water for 20 min then rinsed with water 3 times for 5 min each. Dehydration was performed through grades of ethanol (50%-100%). After dehydration, samples were infiltrated with acetonitrile and embedded in resin. Ultra-thin sections (60 nm) were cut using Leica UC7 ultramicrotome (Leica Microsystems Inc.) and visualized under the Tecnai T12 transmission electron microscope (ThermoFisher Scientific) at an accelerating voltage of 80 kV.

Quantification and statistical analysis

Data sets were analyzed by the Student's t test according to the experiment using GraphPad Prism software (www.graphpad.com), unless otherwise described in the methods or figure legends. Error bars in figures indicate standard deviation (SD) for the number of replicates, as indicated in the figure legend. A p-value less than 0.05 (*), 0.01 (**) or 0.0001 (***) was considered statistically significant.

Acknowledgments

We thank Dr. Qi Zeng for providing antibodies against PTP4A1 and PTP4A2. This work was supported in part by NIH RO1CA069202 and the Robert C. and Charlotte Anderson Chair Endowment.

Disclosure statement

The authors declare no competing interests.

Funding

This work was supported in part by NIH RO1CA069202 and the Robert C. and Charlotte Anderson Chair Endowment.

Data availability

The authors declare that data supporting the findings of this study are available within the Figures and Supplementary Materials of the

manuscript. All raw data associated with Figures and Extended Data are available upon request from the corresponding authors.

References

[1] Attwood MM, Fabbro D, Sokolov AV, et al. Trends in kinase drug discovery: targets, indications and inhibitor design. Nat Rev Drug Discov. 2021;20:839–861.

[2] Bessette DC, Qiu D, Pallen CJ. PRL PTPs: mediators and markers of cancer progression. Cancer Metastasis Rev. 2008;27(2):231–252.

[3] Frankson R, Yu ZH, Bai Y, et al. Therapeutic targeting of oncogenic tyrosine phosphatases. Cancer Res. 2017;77:5701–5705.

[4] Stephens BJ, Han H, Gokhale V, et al. PRL phosphatases as potential molecular targets in cancer. Mol Cancer Ther. 2005;4:1653–1661.

[5] Achiwa H, Lazo JS. PRL-1 tyrosine phosphatase regulates c-Src levels, adherence, and invasion in human lung cancer cells. Cancer Res. 2007;67:643–650.

[6] Fiordalisi JJ, Keller PJ, Cox AD. PRL tyrosine phosphatases regulate rho family GTPases to promote invasion and motility. Cancer Res. 2006;66:3153–3161.

[7] Liang F, Kumar S, Zhang ZY. Proteomic approaches to studying protein tyrosine phosphatases. Mol Biosyst. 2007;3:308–316.

[8] Sun JP, Luo Y, Yu X, et al. Phosphatase activity, trimerization, and the C-terminal polybasic region are all required for PRL1-mediated cell growth and migration. J Biol Chem. 2007;282:29043–29051.

[9] Wang Y, Lazo JS. Metastasis-associated phosphatase PRL-2 regulates tumor cell migration and invasion. Oncogene. 2012;31:818–827.

[10] Wu X, Zeng H, Zhang X, et al. Phosphatase of regenerating liver-3 promotes motility and metastasis of mouse melanoma cells. Am J Pathol. 2004;164():2039–2054.

[11] Zeng Q, Dong JM, Guo K, et al. PRL-3 and PRL-1 promote cell migration, invasion, and metastasis. Cancer Res. 2003;63:2716–2722.

[12] Kato H, Semba S, Miskad UA, et al. High expression of PRL-3 promotes cancer cell motility and liver metastasis in human colorectal cancer: a predictive molecular marker of metachronous liver and lung metastases. Clin Cancer Res. 2004;10:7318–7328.

[13] Saha S, Bardelli A, Buckhaults P, et al. A phosphatase associated with metastasis of colorectal cancer. Science. 2001;294 (5545):1343–1346.

[14] Hardy S, Kostantin E, Hatzihristidis T, et al. Physiological and oncogenic roles of the PRL phosphatases. FEBS J. 2018;285 (21):3886–3908.

[15] Dong Y, Zhang L, Bai Y, et al. Phosphatase of regenerating liver 2 (PRL2) deficiency impairs Kit signaling and spermatogenesis. J Biol Chem. 2014;289(6):3799–3810.

[16] Dong Y, Zhang L, Zhang S, et al. Phosphatase of regenerating liver 2 (PRL2) is essential for placental development by down-regulating PTEN (phosphatase and tensin homologue deleted on chromosome 10) and activating Akt protein. J Biol Chem. 2012;287(38):32172–32179.

[17] Kobayashi M, Bai Y, Dong Y, et al. PRL2/PTP4A2 phosphatase is important for hematopoietic stem cell self-renewal. Stem Cells. 2014;32(7):1956–1967.

[18] Li Q, Bai Y, Lyle LT, et al. Mechanism of PRL2 phosphatase-mediated PTEN degradation and tumorigenesis. Proc Natl Acad Sci U S A. 2020;117(34):20538–20548.

[19] Huang YH, Al-Aidaroos AQ, Yuen HF, et al. A role of autophagy in PTP4A3-driven cancer progression. Autophagy. 2014;10 (10):1787–1800.

[20] Yang Z, Klionsky DJ. Eaten alive: a history of macroautophagy. Nat Cell Biol. 2010;12(9):814–822.

[21] Rabinowitz JD, White E. Autophagy and metabolism. Science. 2010;330(6009):1344–1348.

[22] Papadopoulos C, Meyer H. Detection and clearance of damaged lysosomes by the endo-lysosomal damage response and lysophagy. Curr Biol. 2017;27(24):R1330–R41.

[23] Maejima I, Takahashi A, Omori H, et al. Autophagy sequesters damaged lysosomes to control lysosomal biogenesis and kidney injury. EMBO J. 2013;32(17):2336–2347.

[24] Hung YH, Chen LM, Yang JY, et al. Spatiotemporally controlled induction of autophagy-mediated lysosome turnover. Nat Commun. 2013;4(1):2111.

[25] Dupont N, Lacas-Gervais S, Bertout J, et al. Shigella phagocytic vacuolar membrane remnants participate in the cellular response to pathogen invasion and are regulated by autophagy. Cell Host Microbe. 2009;6(2):137–149.

[26] van den Boom J, Meyer H. VCP/p97-mediated unfolding as a principle in protein homeostasis and signaling. Mol Cell. 2018;69(2):182–194.

[27] Meyer H, Bug M, Bremer S. Emerging functions of the VCP/p97 AAA-ATPase in the ubiquitin system. Nat Cell Biol. 2012;14 (2):117–123.

[28] Franz A, Ackermann L, Hoppe T. Create and preserve: proteostasis in development and aging is governed by Cdc48/p97/VCP. Biochim Biophys Acta. 2014;1843(1):205–215.

[29] Buchan JR, Kolaitis R-M, Taylor JP, et al. Eukaryotic stress granules are cleared by autophagy and Cdc48/VCP function. Cell. 2013;153(7):1461–1474.

[30] AE J, Shu H, AG H, et al. VCP-dependent muscle degeneration is linked to defects in a dynamic tubular lysosomal network in vivo. Elife. 2015;4:e07366.

[31] Papadopoulos C, Kirchner P, Bug M, et al. VCP/p97 cooperates with YOD1, UBXD1 and PLAA to drive clearance of ruptured lysosomes by autophagy. EMBO J. 2017;36:135–150.

[32] Ritz D, Vuk M, Kirchner P, et al. Endolysosomal sorting of ubiquitylated caveolin-1 is regulated by VCP and UBXD1 and impaired by VCP disease mutations. Nat Cell Biol. 2011;13:1116–1123.

[33] Tanaka A, Cleland MM, Xu S, et al. Proteasome and p97 mediate mitophagy and degradation of mitofusins induced by Parkin. J Cell Biol. 2010;191:1367–1380.

[34] Egerton M, Samelson LE. Biochemical characterization of valosin-containing protein, a protein tyrosine kinase substrate in hematopoietic cells. J Biol Chem. 1994;269:11435–11441.

[35] Pham ML, Leister T, Nguyen HA, et al. Immobilization of β-galactosidases from lactobacillus on chitin using a chitin-binding domain. J Agric Food Chem. 2017;65(14):2965–2976.

[36] Li G, Zhao G, Schindelin H, et al. Tyrosine phosphorylation of ATPase p97 regulates its activity during ERAD. Biochem Biophys Res Commun. 2008;375:247–251.

[37] Zhao G, Zhou X, Wang L, et al. Studies on peptide:N-glycanase-p97 interaction suggest that p97 phosphorylation modulates endoplasmic reticulum-associated degradation. Proc Natl Acad Sci U S A. 2007;104:8785–8790.

[38] Allen MD, Buchberger A, Bycroft M. The PUB domain functions as a p97 binding module in human peptide N-glycanase. J Biol Chem. 2006;281:25502–25508.

[39] Kern M, Fernandez-Saiz V, Schafer Z, et al. UBXD1 binds p97 through two independent binding sites. Biochem Biophys Res Commun. 2009;380:303–307.

[40] Qiu L, Pashkova N, Walker JR, et al. Structure and function of the PLAA/Ufd3-p97/Cdc48 complex. J Biol Chem. 2010;285:365–372.

[41] Ju JS, Weihl CC. p97/VCP at the intersection of the autophagy and the ubiquitin proteasome system. Autophagy. 2010;6:283–285.

[42] Chapman E, Maksim N, de la Cruz F, et al. Inhibitors of the AAA + chaperone p97. Molecules. 2015;20:3027–3049.

[43] Magnaghi P, D'Alessio R, Valsasina B, et al. Covalent and allosteric inhibitors of the ATPase VCP/p97 induce cancer cell death. Nat Chem Biol. 2013;9:548–556.

[44] Wang J, Kirby CE, Herbst R. The tyrosine phosphatase PRL-1 localizes to the endoplasmic reticulum and the mitotic spindle and is required for normal mitosis. J Biol Chem. 2002;277:46659–46668.

[45] Zeng Q, Si X, Horstmann H, et al. Prenylation-dependent association of protein-tyrosine phosphatases PRL-1, −2, and −3 with the plasma membrane and the early endosome. J Biol Chem. 2000;275:21444–21452.
[46] Gjorloff-Wingren A, Saxena M, Han S, et al. Subcellular localization of intracellular protein tyrosine phosphatases in T cells. Eur J Immunol. 2000;30:2412–2421.
[47] Cates CA, Michael RL, Stayrook KR, et al. Prenylation of oncogenic human PTPcaax protein tyrosine phosphatases. Cancer Lett. 1996;110(1–2):49–55.
[48] Yoshida Y, Yasuda S, Fujita T, et al. Ubiquitination of exposed glycoproteins by SCF(FBXO27) directs damaged lysosomes for autophagy. Proc Natl Acad Sci U S A. 2017;114:8574–8579.
[49] Fujita N, Morita E, Itoh T, et al. Recruitment of the autophagic machinery to endosomes during infection is mediated by ubiquitin. J Cell Biol. 2013;203:115–128.
[50] Rogov V, Dotsch V, Johansen T, et al. Interactions between autophagy receptors and ubiquitin-like proteins form the molecular basis for selective autophagy. Mol Cell. 2014;53:167–178.
[51] Shaid S, Brandts CH, Serve H, et al. Ubiquitination and selective autophagy. Cell Death Differ. 2013;20:21–30.
[52] Wang Y, Satoh A, Warren G, et al. VCIP135 acts as a deubiquitinating enzyme during p97-p47-mediated reassembly of mitotic Golgi fragments. J Cell Biol. 2004;164:973–978.
[53] Kimura T, Takabatake Y, Takahashi A, et al. Autophagy protects the proximal tubule from degeneration and acute ischemic injury. J Am Soc Nephrol. 2011;22:902–913.
[54] Petejova N, Martinek A. Acute kidney injury due to rhabdomyolysis and renal replacement therapy: a critical review. Crit Care. 2014;18:224.
[55] Nakamura S, Shigeyama S, Minami S, et al. LC3 lipidation is essential for TFEB activation during the lysosomal damage response to kidney injury. Nat Cell Biol. 2020;22:1252–1263.
[56] Settembre C, Di Malta C, Polito VA, et al. TFEB links autophagy to lysosomal biogenesis. Science. 2011;332:1429–1433.
[57] Sardiello M, Palmieri M, Di Ronza A, et al. A gene network regulating lysosomal biogenesis and function. Science. 2009;325:473–477.
[58] Wang H, Quah SY, Dong JM, et al. PRL-3 down-regulates PTEN expression and signals through PI3K to promote epithelial-mesenchymal transition. Cancer Res. 2007;67:2922–2926.
[59] Guo K, Li J, Tang JP, et al. Catalytic domain of PRL-3 plays an essential role in tumor metastasis: formation of PRL-3 tumors inside the blood vessels. Cancer Biol Ther. 2004;3:945–951.
[60] Anderson DJ, Le Moigne R, Djakovic S, et al. Targeting the AAA ATPase p97 as an approach to treat cancer through disruption of protein homeostasis. Cancer Cell. 2015;28:653–665.
[61] Deshaies RJ. Proteotoxic crisis, the ubiquitin-proteasome system, and cancer therapy. BMC Biol. 2014;12:94.
[62] Tang WK, Xia D. Mutations in the human AAA+ Chaperone p97 and related diseases. Front Mol Biosci. 2016;3:79.
[63] Meyer H, Weihl CC. The VCP/p97 system at a glance: connecting cellular function to disease pathogenesis. J Cell Sci. 2014;127:3877–3883.
[64] Bodnar NO, Rapoport TA. Molecular mechanism of substrate processing by the Cdc48 ATPase Complex. Cell. 2017;169:722–735.
[65] Bug M, Meyer H. Expanding into new markets–VCP/p97 in endocytosis and autophagy. J Struct Biol. 2012;179:78–82.
[66] Tresse E, Salomons FA, Vesa J, et al. VCP/p97 is essential for maturation of ubiquitin-containing autophagosomes and this function is impaired by mutations that cause IBMPFD. Autophagy. 2010;6:217–227.
[67] Ju JS, Fuentealba RA, Miller SE, et al. Valosin-containing protein (VCP) is required for autophagy and is disrupted in VCP disease. J Cell Biol. 2009;187:875–888.
[68] Hänzelmann P, Schindelin H. The interplay of cofactor interactions and post-translational modifications in the regulation of the AAA+ ATPase p97. Front Mol Biosci. 2017;4:21.
[69] Zhao G, Li G, Schindelin H, et al. An Armadillo motif in Ufd3 interacts with Cdc48 and is involved in ubiquitin homeostasis and protein degradation. Proc Natl Acad Sci U S A. 2009;106:16197–16202.
[70] Mori-Konya C, Kato N, Maeda R, et al. p97/valosin-containing protein (VCP) is highly modulated by phosphorylation and acetylation. Genes Cells. 2009;14:483–497.
[71] Ariosa AR, Lahiri V, Lei Y, et al. A perspective on the role of autophagy in cancer. Biochim Biophys Acta Mol Basis Dis. 2021;1867:166262.
[72] Mowers EE, Sharifi MN, Macleod KF. Autophagy in cancer metastasis. Oncogene. 2017;36:1619–1630.
[73] Amaravadi RK, Kimmelman AC, Debnath J. Targeting autophagy in cancer: recent advances and future directions. Cancer Discov. 2019;9:1167–1181.
[74] Suzuki T, Park H, Kitajima K, et al. Peptides glycosylated in the endoplasmic reticulum of yeast are subsequently deglycosylated by a soluble peptide: n-glycanase activity. J Biol Chem. 1998;273:21526–21530.
[75] Kirisako T, Kamei K, Murata S, et al. A ubiquitin ligase complex assembles linear polyubiquitin chains. EMBO J. 2006;25:4877–4887.
[76] Li J, Guo K, Koh VW, et al. Generation of PRL-3- and PRL-1-specific monoclonal antibodies as potential diagnostic markers for cancer metastases. Clin Cancer Res. 2005;11:2195–2204.
[77] Agazie YM, Hayman MJ. Development of an efficient "substrate-trapping" mutant of Src homology phosphotyrosine phosphatase 2 and identification of the epidermal growth factor receptor, Gab1, and three other proteins as target substrates. J Biol Chem. 2003;278:13952–13958.
[78] Lam SS, Martell JD, Kamer KJ, et al. Directed evolution of APEX2 for electron microscopy and proximity labeling. Nat Methods. 2015;12:51–54.
[79] Boersema PJ, Raijmakers R, Lemeer S, et al. Multiplex peptide stable isotope dimethyl labeling for quantitative proteomics. Nat Protoc. 2009;4:484–494.
[80] Wang WQ, Bembenek J, Gee KR, et al. Kinetic and mechanistic studies of a cell cycle protein phosphatase Cdc14. J Biol Chem. 2004;279:30459–30468.
[81] Johnson KA. New standards for collecting and fitting steady state kinetic data. Beilstein J Org Chem. 2019;15:16–29.